The 1988 Institute of Metals Lecture
The Minerals, Metals & Materials Society

Mechanical Properties of Thin Films

WILLIAM D. NIX
R.F. Mehl Medalist

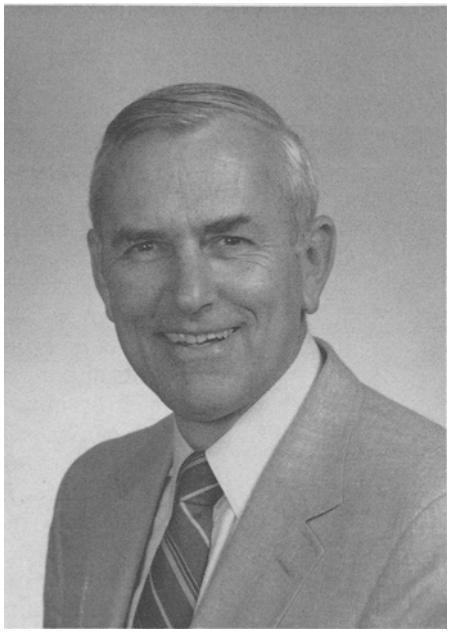

The mechanical properties of thin films on substrates are described and studied. It is shown that very large stresses may be present in the thin films that comprise integrated circuits and magnetic disks and that these stresses can cause deformation and fracture to occur. It is argued that the approaches that have proven useful in the study of bulk structural materials can be used to understand the mechanical behavior of thin film materials. Understanding the mechanical properties of thin films on substrates requires an understanding of the stresses in thin film structures as well as a knowledge of the mechanisms by which thin films deform. The fundamentals of these processes are reviewed. For a crystalline film on a nondeformable substrate, a key problem involves the movement of dislocations in the film. An analysis of this problem provides insight into both the formation of misfit dislocations in epitaxial thin films and the high strengths of thin metal films on substrates. It is demonstrated that the kinetics of dislocation motion at high temperatures are especially important to the understanding of the formation of misfit dislocations in heteroepitaxial structures. The experimental study of mechanical properties of thin films requires the development and use of nontraditional mechanical testing techniques. Some of the techniques that have been developed recently are described. The measurement of substrate curvature by laser scanning is shown to be an effective way of measuring the biaxial stresses in thin films and studying the biaxial deformation properties at elevated temperatures. Submicron indentation testing techniques, which make use of the Nanoindenter, are also reviewed. The mechanical properties that can be studied using this instrument are described, including hardness, elastic modulus, and time-dependent deformation properties. Finally, a new testing technique involving the deflection of microbeam samples of thin film materials made by integrated circuit manufacturing methods is described. It is shown that both elastic and plastic properties of thin film materials can be measured using this technique.

The Institute of Metals Lecture was established in 1921, at which time the Institute of Metals Division was the only professional division within the American Institute of Mining and Metallurgical Engineers Society. It has been given annually since 1922 by distinguished men from this country and abroad. Beginning in 1973 and thereafter, the person selected to deliver the lecture will be known as the "Institute of Metals Division Lecturer and R.F. Mehl Medalist" for that year.

WILLIAM D. NIX, Professor, obtained his B.S. degree in Metallurgical Engineering from San Jose State University, San Jose, CA, and his M.S. and Ph.D. degrees in Metallurgical Engineering and Materials Science, respectively, from Stanford University, Stanford, CA. He joined the faculty at Stanford in 1963 and was appointed Professor in 1972. In 1964, Professor Nix received the Western Electric Fund Award for Excellence in Engineering Instruction and, in

1970, the Bradley Stoughton Teaching Award of ASM. He received the 1979 Champion Herbert Mathewson Award and, in 1988, was the Institute of Metals Lecturer and recipient of the Robert Franklin Mehl Award of TMS-AIME. He was elected Fellow of the American Society for Metals in 1978 and elected Fellow of TMS-AIME in 1988. He also received a Distinguished Alumnus Award from San Jose State University in 1980, and he served as Chairman of the 1985 Gordon Conference on Physical Metallurgy. In 1987, he was elected to the National Academy of Engineering. In 1966, he participated in the Ford Foundation's "Residence in Engineering Practice" program as Assistant to the Director of Technology at the Stellite Division of Union Carbide Corporation. From 1968 to 1970, Professor Nix was Director of Stanford's Center for Materials Research. Professor Nix is engaged in research on the mechanical properties of solids. He is principally concerned with the relation between structure and mechanical properties of materials in both thin film and bulk form. He is coauthor of about 190 publications in these and related fields. Professor Nix teaches courses on dislocation theory and mechanical properties of materials. He is coauthor of "The Principles of Engineering Materials," published in 1973 by Prentice-Hall, Incorporated, Englewood Cliffs, NJ.

I. DEDICATION

THIS paper is dedicated to the memory of Professor G. Marshall Pound, who passed away in May of 1988, during the time this manuscript was being prepared. Professor Pound was Professor of Metallurgy and Materials Science for almost 40 years, having served on the faculties of the Carnegie Institute of Technology and Stanford University. He will be remembered for the gusto he brought to classroom teaching, for his vigorous pursuit of excellence in research, and for the wisdom he provided in the guidance of students and junior faculty (including the present author). His own Institute of Metals Lecture entitled "Perspectives on Nucleation" was published in this journal in April of 1985. It was a fitting tribute to his professional career and to his scholarly work in the field of Metallurgy and Materials Science. The passing of Professor Pound represents a significant loss for the field of Metallurgy and Materials Science and for the departments at Carnegie Mellon and Stanford. But our field and our departments are much richer for the 40-year association we had with this great man.

II. INTRODUCTION

Understanding the relationships between microstructure and mechanical properties has always been one of the primary goals of metallurgy and materials science. Since ancient times, materials have been used primarily for structural, load-bearing applications; thus, the mechanical properties of structural materials have always been of paramount importance to our society. This focus on understanding the mechanical properties of structural materials has stimulated a large amount of research that has led to a deep understanding of the microscopic processes responsible for the mechanical behavior of materials. It has also led to the development of an impressive array of advanced, high-performance structural materials.

In recent years, more and more attention has been devoted to materials that are not intended for use in load-bearing applications. These are the "high-tech" materials that have provided the basis for the information revolution. Too frequently, however, we think of these materials solely in terms of their electronic, magnetic, or optical properties. We need to remind ourselves that other, nonelectronic properties of these materials can be equally important. For example, the materials used to fabricate microelectronic integrated circuits and magnetic disks must perform their electronic and magnetic functions, but they must also have certain chemical and mechanical properties to be able to do this. These devices must be reliable, they must have structural integrity, and they must retain that integrity over their lifetime; corrosive and mechanical failures must not occur. Thus, these materials, though not selected exclusively for their mechanical and chemical properties, must provide adequate resistance to the mechanical and chemical forces that arise in these applications.

Most of the materials and devices that have led to the information revolution are in the form of thin films deposited on rigid substrates. Thin films ranging in thickness from a few nanometers to a few micrometers, for instance, comprise the most important parts of integrated circuits and magnetic disks. As discussed in Section III, these films are frequently subjected to very large stresses which can cause a wide variety of deformation and fracture processes to occur. For these reasons, the mechanical properties of thin films, especially those thin films that are used in integrated circuits and magnetic disks, deserve the same kind of study that the mechanical properties of bulk structural materials have received. Just as for bulk structural materials, it is important to understand the microscopic processes responsible for deformation and fracture of these thin film materials so that the mechanical properties of these materials can be changed through the control of microstructure. These thoughts have motivated much of the work described in this paper.

The viewpoint of this paper is that the field of metallurgy and materials science has the primary responsibility for understanding the mechanical properties of microelectronic and magnetic thin films. In the past, this work has been done largely by scientists and engineers from other disciplines, mainly out of necessity. By contrast, our own field has played a relatively minor role in this work. It is hoped that this paper will encourage others in our field to apply their knowledge and skills in the area of mechanical properties to the problems and opportunities that exist in microelectronic, magnetic, and optical thin film materials.

Following this introduction, we give a brief account of some of the mechanical behavior problems that arise in microelectronic and magnetic thin film materials. This review is purely qualitative and tutorial and provides a technological context for the studies of mechanical properties that are described in the remaining sections of the paper. Following this, a brief description of some of the basic concepts relating to stresses and deformation processes in thin films on substrates are given. This background is provided for those readers who are unfamiliar with the field of thin film mechanical properties.

The remaining sections of the paper deal with selected topics relating to the mechanical properties of thin films on substrates. The subject is much too broad and extensive to attempt a comprehensive review here. Selected topics are presented that relate directly to dislocation

processes in thin films and provide understanding of both the formation of misfit dislocations in thin film structures and the strength of thin films on substrates. Because experimental techniques for measuring stresses and mechanical properties in thin films are just now emerging, it seems appropriate to focus some of our attention on these techniques.

We begin this study by examining the problem of misfit dislocation formation in epitaxial thin films on single-crystal substrates. This problem is important in its own right because there is a great amount of interest in creating device-quality semiconductor alloys by forming epitaxial thin films on dislocation-free silicon substrates. This subject is also of interest here because it provides a vehicle for understanding how dislocation motion occurs in thin films on substrates, which, in turn, leads to an understanding of the high biaxial yield strengths of these films. Our study of the strength of thin films on substrates focuses special attention on the substrate curvature technique for studying these properties. The mechanical properties of thin films can also be studied using submicron indentation methods. This technique has become popular in recent years because of the availability of commercial depth-sensing instruments with sufficient resolution to study the properties of very thin films on substrates.

In the last section of the paper, we report briefly on the development of a new microbeam deflection technique for studying the mechanical properties of thin film materials. This technique makes use of integrated circuit manufacturing methods to create miniature test samples that can be loaded with an indentation instrument. The creation of special test geometries permits the study of deformation in other than the indentation mode (without the hydrostatic pressure that is a natural part of indentation). This approach may also permit a study of fracture and interfacial decohesion of thin films from their substrates.

III. STRESS AND MECHANICAL BEHAVIOR PROBLEMS IN MICROELECTRONIC AND MAGNETIC THIN FILM MATERIALS

As noted in the Introduction, the mechanical properties of thin films have become important in recent years because of the extensive use of these materials in integrated circuits and magnetic disks. In this part of the paper, we cite some of the mechanical behavior problems that arise in these applications.

A. *Microelectronic Integrated Circuit Materials*

In this section of the paper, we examine some of the stress and mechanical behavior problems that arise in integrated circuit structures, such as the complementary metal-oxide semiconductor (CMOS) transistor.

1. *CMOS transistor materials*

Figure 1 shows a schematic picture of the thin film materials and geometries that are used in CMOS transistor devices. The materials are in thin film form, with thicknesses ranging from a few nanometers to about a micrometer. The complex shapes in these structures are also illustrated. It should be noted that a wide variety of materials with very different physical, thermal, and mechanical properties are used to create this structure. The materials include semiconductors (which comprise the active part of the device), metals (which serve as conductors to carry current from one part of the structure to another), thermally grown SiO_2, passivation glasses, and other dielectric materials. These latter materials ensure electrical isolation of one part of the structure from another and in some cases, provide mechanical protection for the underlying, electrically active materials. Note that single crystals and polycrystalline and amorphous phase materials are present.

2. *Stresses in integrated circuit structures*

Typically, CMOS structures are made by growing or depositing the various thin films onto a substrate of single-crystal silicon (a silicon wafer). Because many of these processes occur at elevated temperatures and because some of the materials have differing thermal expansion coefficients, it follows that very large thermal stresses are induced in these materials during manufacture and remain there during the subsequent use of the devices. Thermal stresses of the order of 0.5 GPa are not uncommon. Additional stresses are produced by nonequilibrium growth processes. Most of the growth and deposition processes take place far from thermodynamic equilibrium, with the consequence that highly nonequilibrium microstructures are created. These nonequilibrium microstructures lead to additional stresses caused by the tendency of the film to shrink or expand once it has been deposited onto its substrate. These are sometimes called "intrinsic stresses" in the literature. It is preferable to avoid the implication that bodies can subject themselves to uniform internal stresses and to use the term "growth stresses" instead. Because some of the interfaces are either fully or partially coherent, coherency stresses may also be present in these thin film structures.

3. *Integrated circuit failure processes*

For all of the reasons described above, extremely high stresses are commonly present in integrated circuit structures. It follows that these high stresses cause deformation and, sometimes, fracture to occur in these materials. It is important to understand the mechanisms that control the mechanical properties of these materials so that integrated circuit structures can be designed for mechanical reliability as well as for electronic device performance.

Even elastic deformation of the thin films in integrated circuit structures can represent a kind of failure. The dimensional tolerances associated with the manufacture of these structures must be very small in order to achieve the small feature sizes needed for high density memory. The patterning of these features must be very precise. Very large thin film stresses can change the dimensions of the silicon wafer during processing, making this high dimensional accuracy difficult to achieve. This would be particularly troublesome if the stresses and distortions were not predictable.

a. *Passivation and interconnect failures*

When plastic deformation occurs in interconnect metals, a variety of unwanted effects can occur. Two of these, shown schematically in Figure 2, illustrate that

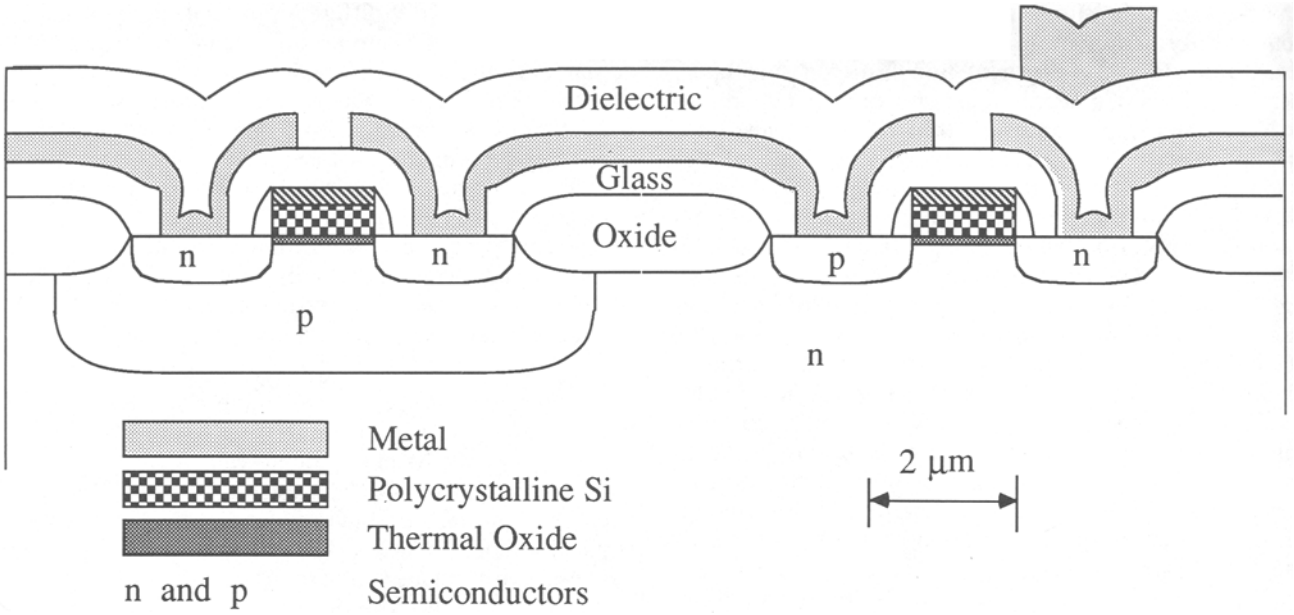

Fig. 1—Cross-sectional structure of a CMOS transistor. The small dimensions of these films and the wide variety of materials involved should be noted. High stresses are present in these films as a result of differences of thermal expansion and of nonequilibrium growth and deposition.

inhomogeneous deformation can cause fracture of the passivation to occur, either by dislocation slip or by grain-boundary sliding. This fracture, in turn, can cause electrical shorts to occur in the circuit if two metallization layers are allowed to come into contact, or it may lead to some form of delayed failure of the interconnect metal. Such delayed failures might involve either corrosion of the interconnect metal or electromigration (a process of diffusional transport of matter in the interconnect line caused by a very high current density).

One of the purposes of the passivation glass is to constrain the underlying metal layer from deforming by diffusional processes. A crack in the passivation removes the constraint at that location and can allow a net flux of interconnect material to flow to that area, leaving a material deficiency elsewhere in the interconnect line. This has two negative consequences. First, the point of material deficiency usually contains voids or cracks that can lead to premature failure of the interconnect. Second, the protrusion of the interconnect material through the crack in the passivation can cause shorts to develop between one metal layer and another. All of these failure processes are initiated by inhomogeneous plastic deformation in the interconnect metal. Needless to say, it is important to understand these deformation processes so that more failure-resistant microstructures can be designed.

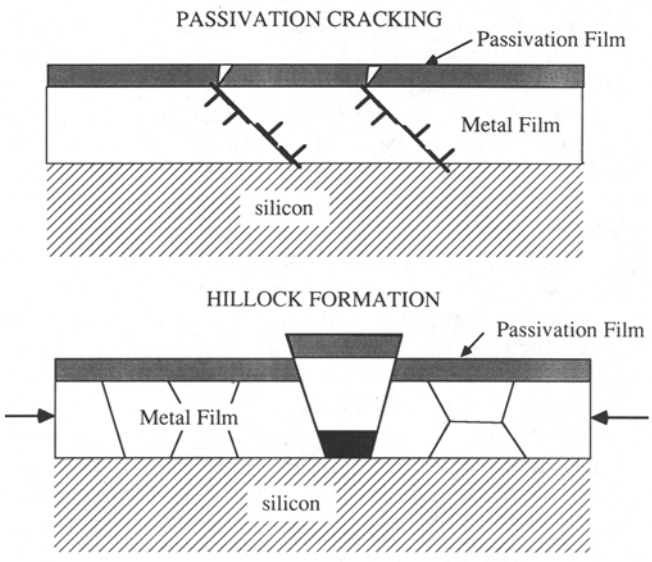

Fig. 2—Mechanisms of inhomogeneous deformation in thin films leading to cracking of the associated passivation film. Dislocation pileups can cause passivation cracking, and grain-boundary sliding can cause hillock formation. Cracking of the passivation film can lead to other failure mechanisms.

b. *Substrate failures*

The thin film stresses represent forces that must be balanced by stresses in the substrate. Because the substrates are usually extremely thick compared to the films, the stresses in the substrate are usually quite small and often negligible. However, this is not always the case. In some cases, the compressive stresses in dielectric films can be so great that the corresponding tensile stresses in the uppermost layer of the substrate can cause dislocations to be nucleated there. Even cracking of the substrate can occur, especially if notches are present in the structure. Figure 3 illustrates the conditions that can lead to substrate cracking. Here, the passivation material is in a state of biaxial compression, which causes bending of the substrate to occur. These bending stresses in the substrate are tensile just beneath the passivation film. The stresses at the notch in the substrate can be sufficiently high either to nucleate dislocations there or perhaps to initiate fracture. The compressive passivation in the notch itself also serves to create a high tensile stress in the substrate, and this further increases the likelihood of crack initiation. The high aspect ratio trench structures that are now being used in some devices are examples of structures that might be susceptible to this kind of mechanical failure.

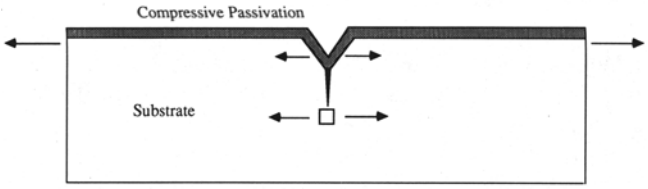

Fig. 3—Substrate cracking caused by stresses in a passivation film; the stresses in the substrate are concentrated at notches.

B. *Magnetic Disk Materials*

Magnetic hard disks are also composed of thin film structures, and, thus, the mechanical properties of the films involved are of technological importance. Here we describe the materials that are used in these applications and the mechanical forces that can lead to failures.

Two different approaches to hard disk construction are shown in Figure 4. The differences relate primarily to the form of the magnetic media used in the device. In the older, more mature technology, the magnetic media consists of fine magnetic particles dispersed in a resin matrix, whereas in the newer technologies, the magnetic material is in the form of a thin magnetic film. However, the basic operation of the disk is the same. In both cases, the disk is rotated at a high speed (with surface velocities as high as 50 mph!), while the head "flies" aerodynamically just above the surface of the disk (within 2000 Å in the case of thin film media) and "writes" or "reads" information on the disk. The head "writes" information by magnetizing or demagnetizing a small portion of the magnetic material on the disk. It also "reads" the information by sensing the magnetic field of the magnetized portion.

The dimensions of the materials involved, the differences in their physical properties, and the nonequilibrium processes used to fabricate hard disk structures can all lead to stress and mechanical behavior problems that are similar to those that arise in integrated circuit structures. However, the presence of the head, which flies at such a high relative velocity so close to the disk, introduces completely new problems in these devices—the problems of friction and wear. Frequent collisions between the head and the disk cannot be avoided. The magnetic films must be able to withstand this kind of abrasion without losing any of the information stored there. The head also makes a crash landing on the disk each time the device is turned off and a sliding takeoff when the disk is turned on once again. These events also produce friction and wear that may eventually lead to failure.

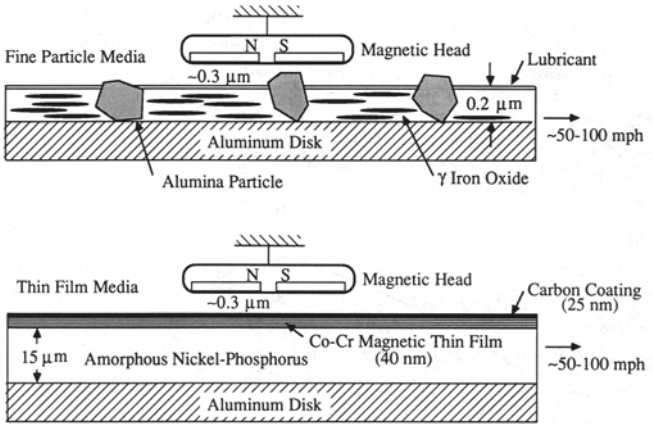

Fig. 4—Illustration of magnetic head-disk interactions. Two types of magnetic media are shown: fine particle media and thin film media. The head "flies" aerodynamically very close to the disk at a very high velocity. Collisions between the head and disk occur frequently.

The purpose of some of the microstructural features in hard disk materials is to provide resistance to friction and wear. The carbon coating on the top of the film is a hard surface with a low coefficient of friction. This permits the head to slide on the surface of the disk without producing mechanical damage. The particles of Al_2O_3 in the fine particle media also provide mechanical durability. During takeoff, landing, and collision events, the head slides on the tops of the particles rather than gouging into the softer matrix containing the magnetic particles. The mechanical properties of all of these submicron features are crucial to the successful performance of these devices. Needless to say, the measurement and understanding of the mechanical properties of these materials is of great importance.

IV. BASIC CONCEPTS AND EQUATIONS RELATING TO STRESSES IN THIN FILMS ON SUBSTRATES

Because much of this paper relates to processes that are driven by the stresses that are present in thin films on substrates, it is important to have a clear understanding of the stress analysis of the thin film/substrate problem. In this section of the paper, we give an elementary treatment of this problem and show how to calculate the stresses in various circumstances and how these stresses lead to elastic bending of the substrate. In Section VI of the paper, we make use of these relations to show how the stress in the film can be determined from a measurement of the substrate curvature. We present this analysis for those readers who have not studied the basic aspects of this problem. More detailed and in-depth treatments can be found in the literature.[1,2,3]

A. *The Mechanics of Stresses in Thin Films on Substrates*

We start by considering a film/substrate composite that is completely free of stress, as shown in Figure 5. We assume that the film is very thin compared to the substrate (thin film approximation), and we also assume that the lateral dimensions of the film and substrate are much greater than their total thickness. Because the film is under no stress, we can imagine removing it from the substrate and allowing it to stand in a stress-free state. In this state, the lateral dimensions of the film will match exactly those of the substrate from which it was removed. If the state of the film is never changed, it can always be reattached to the substrate without causing any stresses to be generated in either the film or substrate. However, if the dimensions of the film change in any way, then elastic strains and stresses will develop when the film is reattached to the substrate. For the present analysis, we consider that the film experiences a uniform

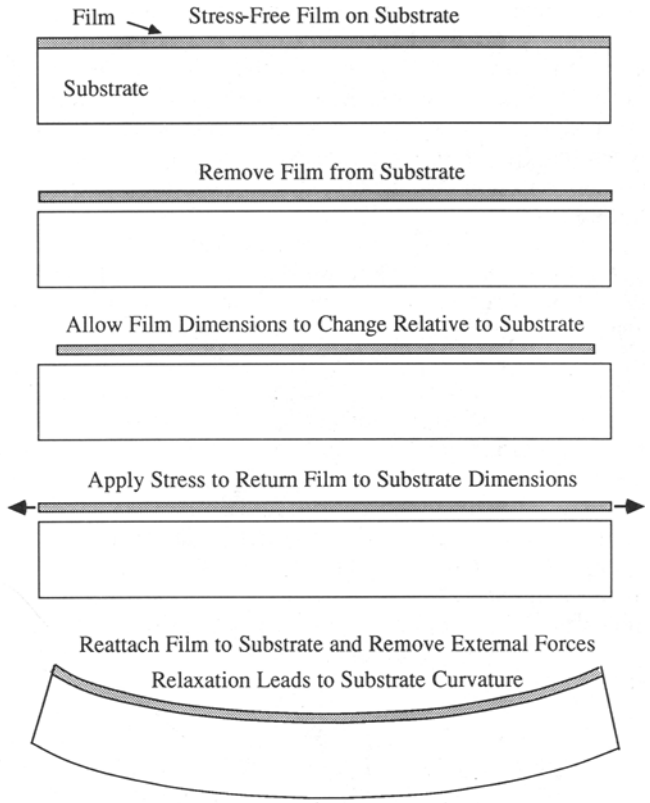

Fig. 5—Illustration of the relationship between the biaxial stress in a thin film and the associated bending of the substrate.

volume change (dilatational transformation strain, e_T) in the detached state. This dilatational strain is measured relative to that of the substrate. This is shown in the figure as a negative dilatation (a volume shrinkage). For a pure dilatational strain, the principal strain components are $\varepsilon_{xx}(T) = \varepsilon_{yy}(T) = \varepsilon_{zz}(T) = e_T/3$. There are many ways in which the volume of a film might change relative to the substrate. For example, if the film and substrate have different thermal expansion coefficients, a change in temperature will produce the relative volume change discussed here. In addition, the annihilations of excess vacancies, dislocations, and grain boundaries are processes that lead to volume changes due to densification. Also, phase transformations and composition changes can produce dilatational strains in the film. For the case of heteroepitaxial films, a natural misfit exists between the film and the substrate in their stress-free state.

We now consider the process of reattaching the film to the substrate. Because the lateral dimensions of the film no longer match those of the substrate, a biaxial stress must be imposed on the film to elastically deform it so that it again fits the dimensions of the substrate. The stress required to do this produces elastic strains, ε_{xx} and ε_{yy}, that compensate exactly these components of the transformation strain. Thus,

$$\varepsilon = \varepsilon_{xx} = \varepsilon_{yy} = -\frac{e_T}{3} \qquad [1]$$

Using Hooke's law, this leads to a biaxial stress in the film:

$$\sigma = \sigma_{xx} = \sigma_{yy} = M\varepsilon \qquad [2]$$

where M is the biaxial elastic modulus of the film. For isotropic elasticity, the biaxial modulus of the film is simply

$$M = \frac{E}{1-\nu} \qquad [3]$$

where E is Young's modulus and ν is Poisson's ratio.

In Figure 5, we note that the tensile forces needed to deform the film to match the dimensions of the substrate produce a biaxial stress state in the film. As long as these forces are present, the stress in the film does not change when it is reattached to the substrate. We now consider the changes that occur when these edge forces are removed after the film is again perfectly bonded to the substrate. A principle of superposition can be used to understand what happens when the edge forces are removed. We remove the forces at the edges by superimposing forces of opposite signs on the edges of the film. These additional forces remove the normal tractions from the edges of the film, and they produce shear stresses on the film/substrate interface near the edges of the film. These shear stresses provide the forces needed to maintain the biaxial stress in the film. These forces also cause the substrate to bend elastically, as discussed below.

B. *Single-Crystal Thin Films*

For the case of single-crystal films or for polycrystalline films with strong crystallographic texture, the anisotropy of the elastic properties must be taken into account. Here we give some results for cubic single-crystal films. For a film in which the (001) cube plane lies parallel to the plane of the film, the biaxial elastic modulus is isotropic in the plane of the film and is given by

$$M\,(001) = C_{11} + C_{12} - \frac{2C_{12}^2}{C_{11}} \qquad [4]$$

where C_{11} and C_{12} are components of the stiffness matrix. We note that neither Young's modulus nor Poisson's ratio alone are isotropic in the (001) plane, but the ratio $E/(1-\nu)$ which forms the biaxial modulus is isotropic in that plane. A single-crystal film with a (111) plane lying in the plane of the film is fully isotropic in that plane. In this case, the biaxial modulus is

$$M\,(111) = \frac{6C_{44}(C_{11} + 2C_{12})}{C_{11} + 2C_{12} + 4C_{44}} \qquad [5]$$

For a single-crystal film with a (011) plane parallel to the plane of the film, the elastic properties are not isotropic in the plane of the film. The elastic moduli in the mutually perpendicular [100] and [01$\bar{1}$] directions are different. If such a film is subjected to in-plane stresses such that the result is an equal biaxial strain, $\varepsilon = \varepsilon_{xx} = \varepsilon_{yy}$, the stresses in the two directions can be computed using the following moduli:

$$M\,[100] = C_{11} + C_{12} - \frac{C_{12}(C_{11} + 3C_{12} - 2C_{44})}{(C_{11} + C_{12} + 2C_{44})} \qquad [6]$$

$$M[01\bar{1}] = \frac{(2C_{11} + 6C_{12} + 4C_{44})}{4} - \frac{(2C_{11} + 2C_{12} - 4C_{44})}{4} \frac{(C_{11} + 3C_{12} - 2C_{44})}{(C_{11} + C_{12} + 2C_{44})} \quad [7]$$

C. *Substrate Bending and Substrate Stresses*

The edge forces exerted on the substrate by the biaxial stress in the film cause the substrate to deform elastically in biaxial bending. The amount of bending depends on the thickness and biaxial elastic modulus of the substrate. If the biaxial elastic modulus is isotropic in the plane of the substrate, as it is for (001) and (111) substrates of cubic materials (*e.g.*, silicon), then the film/substrate composite adopts the shape of a spherical shell when it deforms. A simple biaxial bending analysis shows that the curvature, K, and radius of curvature, $R = K^{-1}$, are given by

$$K = \frac{1}{R} = \frac{1}{M_s} \frac{6\sigma_f h_f}{h_s^2} \quad [8]$$

where $M_s = (E/1 - \nu)_s$ is the biaxial elastic modulus of the substrate, σ_f is the biaxial tensile stress in the film, h_f is the thickness of the film, and h_s is the thickness of the substrate. The edge force per unit length is represented by $\sigma_f h_f$ in this expression. We note that this relation can be inverted to give the stress in the film as a function of the substrate curvature caused by that stress, as shown by

$$\sigma_f = M_s \frac{h_s^2}{6h_f R} \quad [9]$$

For single-crystal substrates, the biaxial elastic modulus, M_s, must be computed from the components of the stiffness matrix for that crystal. The modulus M_s is given by Eqs. [4] and [5] for (001) and (111) substrates, respectively. When the (011) plane is parallel to the plane of the substrate (or for noncubic substrates), the substrate is not elastically isotropic in that plane and does not bend symmetrically.

It should be noted that Eq. [8] for the elastic bending of the substrate does not depend on the elastic properties or any other mechanical properties of the film. The reason for this relates to the thin film approximation that is made in the derivation of this result. Typically, films about 1-μm thick are deposited onto substrates that may be 500 to 1000 times thicker. In such cases, the flexural modulus of the thin film/substrate composite is completely dominated by the properties of the substrate. The properties of the film have a negligible effect on the bending. It follows that when multiple thin films are deposited sequentially onto a much thicker substrate, each film causes a fixed amount of bending to occur, irrespective of the order in which the films are deposited. The amount of curvature change is determined by the stress and thickness of each film. The total change of substrate curvature is simply the sum of the curvature changes associated with the presence of each film. Of course, the sign of the curvature change caused by each film must be taken into account. For cases in which the films are not thin compared to the substrate, a more elaborate bending analysis must be used that takes account of the elastic properties of the films.[3]

It is commonly believed that the stresses in a thin film of uniform thickness can cause significant stresses to develop in the underlying films and in the substrate. Specifically, it is widely assumed that depositing a thin film of a passivation material like Si_3N_4 which typically is in a state of high biaxial compressive stress will cause correspondingly large biaxial tensile stresses to develop in the substrate and in underlying thin films. A simple bending analysis using the thin film approximation shows that this is not true. Although the compressive stress in the passivation film is compensated by tensile stresses in the underlying layers, these tensile stresses are usually extremely small and can often be ignored. Typically, the maximum tensile stress induced in the underlying layers, σ_{induced}, by the compressive stress in the passivation film, $\sigma_{\text{pass.}}$, is given by

$$\sigma_{\text{induced}} = -\frac{3h_p}{h_s} \sigma_{\text{pass.}} \quad [10]$$

This formula is obtained by balancing the force per unit length in the passivation film, $\sigma_{\text{pass.}} h_p$, with an opposing force per unit length and moment per unit length in the substrate. For the typical dimensions of $h_p = 1$ μm and $h_s = 500$ μm, this shows that the magnitude of the stress in the underlying layers is less than 1 pct of the compressive stress in the passivation. For patterned structures, the interaction of stresses in different films can be significant and must be taken into account.

D. *Sources of Strain*

As discussed above, the stresses in thin films on substrates can be viewed as arising from the misfit that must be accommodated elastically when the film is attached to the substrate.

1. *Thermal strains*

There are various types of strains that can develop. For thermal mismatch problems, the elastic strain needed to fit the film to the substrate is

$$\varepsilon = -(\alpha_f - \alpha_s)(T - T_0) = -\Delta\alpha\Delta T \quad [11]$$

where α_f and α_s are the linear thermal expansion coefficients of the film and substrate, respectively, T is the current temperature, and T_0 is the initial temperature at which the film and substrate were in a stress-free state. A typical case is one in which a metal film is deposited onto silicon in a stress-free state at high temperatures and subsequently cooled to room temperature. In such cases, $\alpha_f > \alpha_s$ and $T < T_0$ so that the elastic accommodation strain is positive and tensile stresses are developed in the film.

2. *Growth strains*

As discussed earlier, if the density of the film changes after it has been bonded to the substrate, an "intrinsic"

or growth stress develops in the film. In this case, the elastic accommodation strain is given by

$$\varepsilon = -\frac{e_T}{3} \qquad [12]$$

where e_T is the dilatational "transformation" strain associated with the change in density. A film that densifies when it is attached to the substrate must be subjected to biaxial tensile strain (and corresponding tensile stress) to match the dimensions of the substrate.

3. *Epitaxial strains*

For epitaxial films on thick substrates, the elastic accommodation strain is simply

$$\varepsilon = \frac{\Delta a}{a} \approx \frac{a_s - a_f}{a_f} \approx \frac{a_s - a_f}{a_s} \qquad [13]$$

where a_f and a_s are the lattice parameters of the film and substrate, respectively. Here, all of the elastic accommodation is assumed to take place in the film because the substrate, being so much thicker than the film, is essentially rigid.

V. FORMATION OF MISFIT DISLOCATIONS IN EPITAXIAL THIN FILMS

We begin our study of mechanical properties of thin films on substrates by considering the formation of misfit dislocations in epitaxial thin films on single-crystal substrates. This problem is important in its own right because of the technological interest in forming dislocation-free epitaxial thin films or single-crystal substrates. It is also important because it provides a basis for understanding the dislocation processes responsible for plastic deformation of thin films on nondeformable substrates.

There is a great amount of interest in growing semiconductor thin films on dislocation-free substrates using heteroepitaxy. The basic idea of this technology is that semiconductors that are difficult to grow as bulk crystals might be grown by forming heteroepitaxial layers on dislocation-free single-crystal substrates. Of course, any lattice mismatch between the film and the substrate must be accommodated by a uniform strain in the film (together with slight bending of the substrate), and this typically leads to very large biaxial stresses in the film. Intuitively, one might expect these large stresses to be relaxed by plastic flow in the film (through dislocation nucleation and motion), regardless of the film thickness. But this cannot occur in very thin films because the energies of the dislocations created by such relaxation processes are greater than the recovery of strain energy associated with the relaxation. Thus, there is a critical film thickness, h_c, below which the film is stable with respect to dislocation formation. Below that critical thickness, misfit dislocations cannot and do not form in heteroepitaxial structures.

A. *Equilibrium Theory*

The equilibrium theory of misfit dislocation formation was developed by van der Merwe,[4] Matthews and Blakeslee,[5,6] and Matthews[7] and is now well established. Figure 6 illustrates the essential features of the theory. As shown in the figure, the energy (per unit film area) of a very thin film is lowest when no dislocations are present. Such films are perfectly coherent with the substrate in their equilibrium state and have an energy (per unit area) given by

$$E_{\text{homogeneous}} = Mh\varepsilon^2 \qquad (h < h_c) \qquad [14]$$

where M is the biaxial elastic modulus of the film, h is the film thickness, and ε is the biaxial elastic strain that must be imposed on the film to bring the lattice of the film into coincidence with that of the substrate. We note that $M\varepsilon$ is the biaxial stress in the film. The fact that the equilibrium state for a very thin film is dislocation-free can be shown by considering a slightly thicker film that contains misfit dislocations. The introduction of misfit dislocations partially accommodates the lattice misfit between the film and substrate, and this allows the uniform strain in the film (and its associated energy) to be reduced. When dislocations with Burgers vectors, b, and spacing, S, are formed, the remaining homogeneous strain in the film is $(\varepsilon - b/S)$, and the corresponding strain energy is reduced accordingly. While the strain energy associated with the homogeneous strain decreases as misfit dislocations are introduced, the energies of those dislocations increase the energy of the system. The dislocation energy (per unit area) is expressed approximately as

$$E_{\text{dislocations}} = \frac{\mu b^2}{4\pi(1-\nu)}\frac{2}{S}\ln\left(\frac{\beta h}{b}\right) \qquad [15]$$

where μ is the shear modulus of thin film and substrate (here assumed to be the same), ν is Poisson's ratio, and

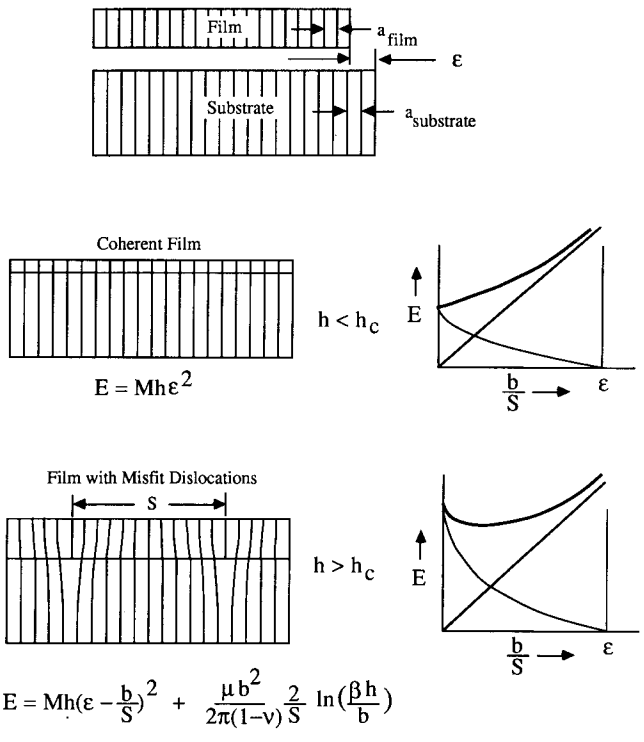

Fig. 6—Illustration of the Matthews and Blakeslee[5,6,7] equilibrium theory of misfit dislocation formation. Below a critical film thickness, the equilibrium state of the film is dislocation-free. Dislocations form in thicker films to reduce the free energy of the system.

β is a numerical constant of the order of unity. The factor $2/S$ in this expression represents the misfit dislocation length per unit film area, while the remaining terms give the energy per unit length of each misfit dislocation. The dislocation energy depends logarithmically on the film thicknesses because this dimension controls the outer cutoff radius for the elastic field of the dislocations. The total energy of thin films containing misfit dislocations is then found by adding these two terms. The result is

$$E = Mh\left(\varepsilon - \frac{b}{S}\right)^2 + \frac{\mu b^2}{4\pi(1-\nu)}\frac{2}{S}\ln\left(\frac{\beta h}{b}\right) \quad [16]$$

We note that the energy associated with the uniform strain (the first term in the right-hand side of Eq. [16]) varies linearly with the film thickness, h, while the energy associated with the misfit dislocation varies only logarithmically with film thickness. As a consequence, only above a critical thickness, h_c, does the introduction of misfit dislocations lead to a decrease in the energy of the system. The equilibrium state of the system can be determined by finding the conditions for which the total energy (per unit area) reaches an absolute minimum with respect to the number of misfit dislocations per unit length, $1/S$. This is obtained by setting the following derivative to zero:

$$\frac{\partial E}{\partial\left(\frac{1}{S}\right)} = -2Mh\mathbf{b}\left(\varepsilon - \frac{b}{S}\right) + \frac{\mu b^2}{2\pi(1-\nu)}\ln\left(\frac{\beta h}{b}\right) = 0 \quad [17]$$

The critical film thickness is then found by solving this equation for the special case of $b/S = 0$:

$$\frac{h_c}{\ln\left(\frac{\beta h_c}{b}\right)} = \frac{\mu b}{4\pi(1-\nu)M\varepsilon} \quad [18]$$

For $h > h_c$, the equilibrium state includes misfit dislocations, as shown in Figure 6, but for $h < h_c$, the lowest energy is achieved when no misfit dislocations are present. Thus, there is a critical thickness below which fully coherent epitaxial films are thermodynamically stable.

B. *Comparison with Experiment*

Recent work on heteroepitaxial films of Si-Ge on Si suggests that these films remain dislocation-free at thicknesses much greater than the critical thickness predicted by the equilibrium theory.[8,9,10] This result is shown in Figure 7 for Si-Ge alloy films on Si substrates. Here, the data of Bean *et al.*[9] are compared with predictions of the equilibrium theory. For films containing 20 pct Ge or less, the actual film thicknesses at which misfit dislocations are observed are an order of magnitude greater than the critical thicknesses predicted by the equilibrium theory. These results have also been found recently by Gronet,[11] as shown in Figure 8. Similar results have been reported by Tsao *et al.*[10] for Ge-Si alloy films on Ge substrates. Some of their results are shown in Figure 9. Although there was some debate about the evidence for this discrepancy,[12,13] it now seems likely that the results

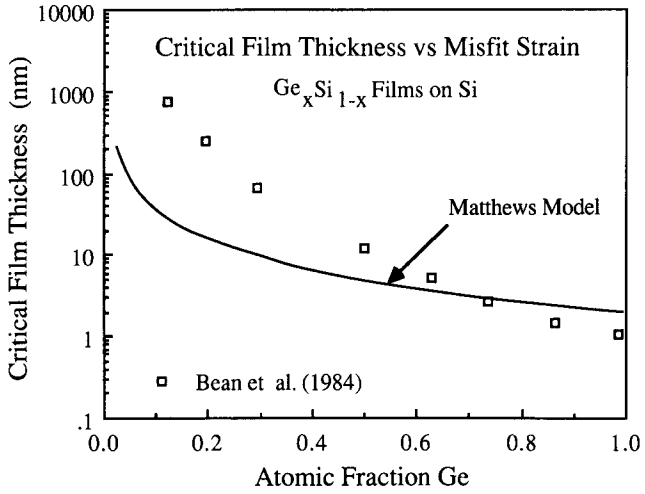

Fig. 7—Critical film thickness as a function of misfit strain for Ge_xSi_{1-x} films on Si substrates. The strain in the film is determined by the composition. The experimental results of Bean *et al.*[9] are compared with Matthews and Blakeslee's equilibrium theory.[5,6,7]

cited here are genuine and that the cause of the discrepancy is related to the kinetics of nucleation, motion, and multiplication of dislocations in epitaxial semiconductor films.[10,14-16] Below, we give a dislocation dynamics model for the formation of misfit dislocations in epitaxial thin films. The model provides a mechanistic understanding of misfit dislocation formation in terms of the kinetics of nucleation, motion, and multiplication of misfit dislocations.

Following the work of Matthews and Blakeslee,[5,6,7] Freund[17] has shown that the most powerful way to understand the formation of misfit dislocations in epitaxial structures is to consider the energetics associated with the incremental extension of a misfit dislocation rather than considering the overall energy change associated with the formation of a periodic array of misfit dislocations. Because this approach is based on the mechanisms of misfit dislocation formation, it is easy to see how the kinetics of dislocation motion should be included in the analysis.

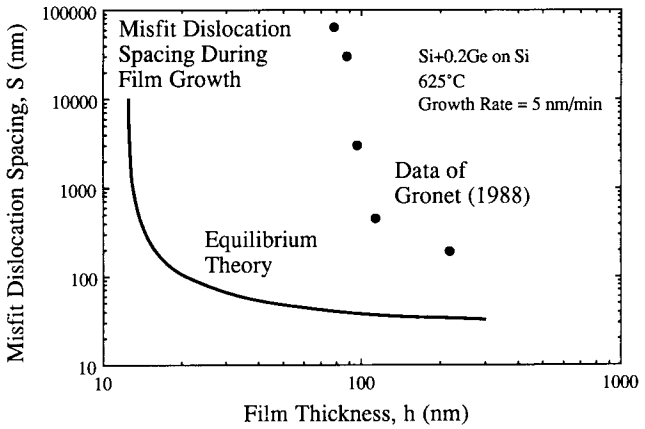

Fig. 8—Misfit dislocation spacing in Si-Ge films on Si substrates as a function of film thickness during film growth. The predictions of the equilibrium theory[5,6,7] are compared with measurements reported by Gronet.[11] The observed spacings are much greater than expected from the equilibrium theory.

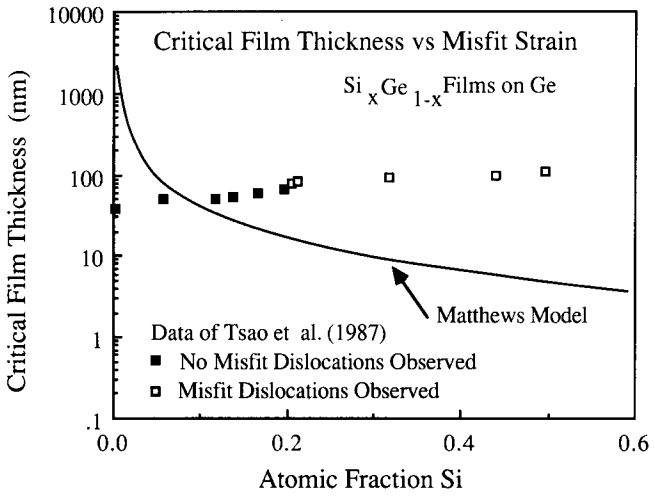

Fig. 9—Critical film thickness as a function of misfit strain (film composition) for Ge-rich films on Ge substrates.[10] The composition (or strain) at which misfit dislocations are first observed is greater than predicted by the equilibrium theory.[5,6,7]

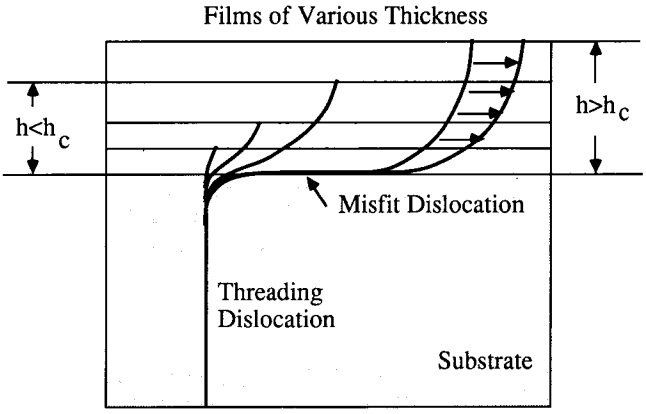

Fig. 11—Bending of a threading dislocation in a strained film growing on a substrate. Above a critical thickness, the strain in the film is sufficient to cause the dislocation in the film to move and create a misfit dislocation.

C. *Mechanisms of Misfit Dislocation Formation*

Following the work of Freund,[17] we envision a dislocation that extends from the free surface of a film to the film-substrate interface and deposits a misfit dislocation at the film/substrate interface as it moves. This is shown in Figure 10. In this figure and throughout this section, we consider the case of fcc crystals with the (001) orientation and focus our attention on the motion of dislocations on the octahedral, {111}, planes. For films of this orientation, the angles defining the {111} slip plane normal and the Burgers vector are $\phi = \cos^{-1}(1/\sqrt{3})$ and $\lambda = \cos^{-1}(1/\sqrt{2})$, respectively. Much of the recent experimental data has been obtained for Si-Ge alloy films grown onto pure Si substrates. Lattice mismatch causes the films to be in a state of biaxial compression, as shown in the figure.

1. *Threading dislocations*

We may ask how the process shown in Figure 10 gets started. If dislocations are present in the substrate on which the film is growing, then they grow naturally into the epitaxial film and reach the free surface of the film. These are sometimes called "threading" dislocations. The process by which threading dislocations can begin to form misfit dislocations at the film/substrate interface is shown schematically in Figure 11. The biaxial stresses in the film exert forces on the threading dislocation and cause it to move in its slip plane. The portion of the dislocation that resides in the substrate remains stationary; the forces on it are much smaller and are of opposite signs. Thus, the threading dislocation in the film bends over as it moves and eventually leaves a misfit dislocation in its wake. Continued movement of the threading dislocation extends the length of the misfit dislocation.

Misfit dislocations are also formed in epitaxial films grown onto dislocation-free substrates. In such cases, threading dislocations are not available to produce the misfit dislocations. Although the process is not well understood, misfit dislocations must be created by some form of dislocation nucleation, most probably at defects at the free surface of the growing film. Figure 12 shows how the nucleation of a dislocation half-loop at the surface of the growing film eventually leads to the formation of a misfit dislocation at the film/substrate interface. The two ends of the half-loop move in opposite directions and create additional misfit dislocation lengths as they move.

2. *Criterion for misfit dislocation formation*

Freund's model of misfit dislocation formation is based on the idea that the work done by the stress in the film

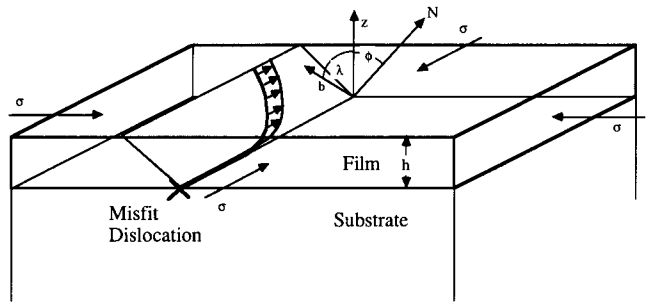

Fig. 10—Dislocation motion in a thin film on a substrate leading to the deposition of a misfit dislocation at the interface between the film and the substrate.

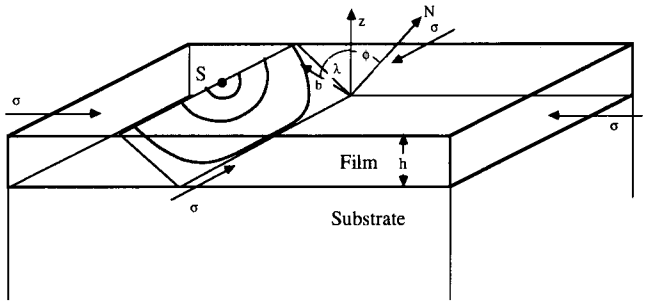

Fig. 12—Dislocation nucleation at the surface of a strained film. The expanding half-loop eventually produces a misfit dislocation at the film-substrate interface.

when the dislocation moves a unit distance must provide enough energy to deposit a unit length of misfit dislocation. Following Freund, we call the work done by the stress in the film W_{layer} and call the work required to form a unit length of dislocation $W_{\text{dislocation}}$. For the dislocation geometry shown in Figure 10, we can show that W_{layer} is

$$W_{\text{layer}} = \frac{\tau bh}{\sin \phi} = \frac{\cos \lambda \cos \phi}{\sin \phi} \sigma bh = \frac{\sigma bh}{2} \qquad [19]$$

For the fcc slip geometry under consideration, the Burgers vector makes an angle of 60 deg to the line of the misfit dislocation; thus, the misfit dislocation deposited at the film/substrate interface is a 60 deg mixed dislocation, and $W_{\text{dislocation}}$ must be found for that case. We use the results of Freund[17] and Barnett[18] for edge and screw dislocations, respectively, to construct the solution for a 60 deg dislocation. Freund has shown that the energy of an edge dislocation lying at the interface between a thin film and semi-infinite substrate can be expressed as

$$W_{\text{edge}} = \frac{b_e^2}{4\pi(1 - \nu)} \frac{2\mu_f \mu_s}{(\mu_f + \mu_s)} \ln \left(\frac{\beta_e h}{b_e}\right) \qquad [20]$$

where (following the form given by Matthews) μ_f and μ_s are the shear moduli of the film and the substrate, respectively, β_e is a numerical constant equal to 0.701, and the other terms have their usual meaning. The result for a screw dislocation was obtained recently by Barnett[18] and takes the similar form

$$W_{\text{screw}} = \frac{b_s^2}{4\pi} \frac{2\mu_f \mu_s}{(\mu_f + \mu_s)} \ln \left(\frac{\beta_s h}{b_s}\right) \qquad [21]$$

where $\beta_s = 1.0$. We can obtain the result for a 60 deg mixed dislocation by noting that $b_e = (\sqrt{3}/2)b$ and $b_s = b/2$ and by adding the energies of the edge and screw components. After some rearrangement and using $\nu = 0.3$, we obtain

$$W_{60\,\text{deg dislocation}} = 0.95 \frac{b^2}{4\pi(1 - \nu)} \frac{2\mu_f \mu_s}{(\mu_f + \mu_s)} \ln \left(\frac{\beta h}{b}\right) \qquad [22]$$

where $\beta = 0.755$.

We may now continue to develop a model for misfit dislocation formation. The value of W_{layer} must be greater than $W_{60\,\text{deg dislocation}}$ in order for the dislocations in the film to move and deposit misfit dislocations. On the basis of this, we may define an effective stress for dislocation motion in terms of the work done by the stress in the film less the work required to deposit the misfit dislocation:

$$\tau_{\text{eff}} b \frac{h}{\sin \phi} = W_{\text{layer}} - W_{60\,\text{deg dislocation}} \qquad [23]$$

This net driving force is positive only at film thicknesses greater than the critical thickness. Indeed, the critical film thickness discussed above can be found by setting the right-hand side of this equation equal to zero.

$$W_{\text{layer}} = W_{60\,\text{deg dislocation}}$$

$$\frac{h_c}{\ln\left(\frac{\beta h_c}{b}\right)} = 1.9 \frac{b}{4\pi(1 - \nu)\sigma} \frac{2\mu_f \mu_s}{(\mu_f + \mu_s)} \qquad [24]$$

where the biaxial stress, σ, has been used in place of the product of the biaxial modulus and misfit strain, $\sigma = M\varepsilon$. This result is a more exact form of Eq. [18] for this particular orientation. This relation may also be used to find the relaxed stress in a film containing an equilibrium number of misfit dislocations. For $h > h_c$, the result is

$$\sigma = \frac{1.9b}{4\pi(1 - \nu)h} \frac{2\mu_f \mu_s}{(\mu_f + \mu_s)} \ln \left(\frac{\beta h}{b}\right) \qquad [25]$$

3. *Kinetics of dislocation motion*

The kinetics of misfit dislocation formation can be predicted using the effective stress defined by Eq. [23] and the dislocation mobility. Haasen and Alexander[19] have measured dislocation mobilities in Si and Ge, and others have made similar measurements for other semiconductors.[20,21] According to these studies, the dislocation velocities in semiconductors can be expressed as

$$v = B \exp\left(-\frac{U}{kT}\right)\left(\frac{\tau_{\text{eff}}}{\tau_0}\right)^{1.2} \qquad [26]$$

where τ_{eff} is the effective stress as defined above, and U is the activation energy for dislocation motion. Because the effective stress is zero at the critical thickness, the rates of dislocation motion and misfit dislocation formation are both zero at $h = h_c$. The dislocations can move with finite velocities only in films that are greater than the critical thickness.

Because each moving dislocation deposits a misfit dislocation as it moves, the overall rate of misfit dislocation formation can be found by multiplying the velocity by the number of moving dislocations per unit area. If the misfit dislocation density, defined as the line length of misfit dislocations per unit area of film, is ρ_{mf}, it follows that the rate of production of misfit dislocations can be expressed as

$$\frac{d\rho_{mf}}{dt} = Nv \qquad [27]$$

where N is the moving dislocation density. Thus, the rate of formation of misfit dislocations depends on the density of mobile dislocations that are already there. If the substrate is dislocation free and no dislocations are nucleated in the epitaxial film during growth, then misfit dislocations cannot form.

a. *Constant threading dislocation density*

The simplest kinetic model is one in which a fixed number of threading dislocations is assumed to exist in the substrate prior to film growth. Such dislocations would extend into the growing film and would be subjected to the stresses there. As the film thickness increases, above the critical film thickness, these dislocations bend over

and begin to glide parallel to the film-substrate interface, creating misfit dislocations as they move. This process is shown in Figure 11. If the density of threading dislocations is constant (no multiplication of existing dislocations or nucleation of new ones), the rate of increase of misfit dislocation line length is governed entirely by the dislocation velocity. If we define the average spacing between misfit dislocations, S, as

$$S = \frac{2}{\rho_{mf}} \qquad [28]$$

then the spacing between misfit dislocations will decrease continuously during the course of growth once the critical film thickness has been exceeded. Figure 13 shows how the misfit dislocation spacing in epitaxial films of Si + 0.2Ge on Si is expected to change during film growth. Various constant mobile dislocation densities were assumed in the calculations. The film was assumed to be growing at a rate of 5 nm/min at a temperature of 625 °C, and the velocities of the dislocations were calculated using Eq. [26] with $U = 2.2$ eV, $\tau_0 = 9.8$ MPa, and $B = 7.33 \times 10^4$ m/s. The curve indicating the largest misfit spacings corresponds to the lowest mobile dislocation density. The lowest curve corresponds to the equilibrium spacing between misfit dislocations. For all curves, the misfit spacings tend toward infinity at a film thickness of about 13.5 nm. This corresponds to the critical film thickness for this system. One notes that the curve corresponding to the largest dislocation density coincides with the equilibrium theory at large film thicknesses, as expected.

b. *Multiplication of dislocations*

The above treatment is unrealistic because it does not allow for either dislocation multiplication or nucleation of new dislocations in the course of growth. Several mechanisms of dislocation multiplication can be envisioned. One of these, suggested first by Hagen and Strunk,[22] has been directly observed by Rajan and Denhoff[23] using weak-beam transmission electron microscopy (TEM) techniques. According to this mechanism, two crossing misfit dislocations with the same Burgers vectors of the kind shown in Figure 14 can annihilate locally and produce two new mobile dislocations, which can then glide and produce additional lengths of misfit dislocation. This is but one of many mechanisms that are possible. All such mechanisms, however, can be described using the concept of a breeding factor. We define the breeding factor, δ, as the number of new dislocations produced per unit length of glide motion by each moving dislocation. Then the multiplication of dislocations can be described by

$$\frac{dN}{dt} = N\delta v \qquad [29]$$

The effect of dislocation multiplication on the misfit dislocation spacing during the course of film growth is shown in Figure 15. Here we have assumed a very low initial dislocation density of $N = 0.1$ cm^{-2} and have considered constant breeding factors of 5, 10, and 20 dislocations/mm. We note that although some dislocation motion occurs as soon as the critical film thickness is exceeded, the misfit dislocation spacing remains very large until the film has reached a thickness of about 100 nm. The predictions are in qualitative agreement with the results of Gronet[11] shown in Figure 8.

According to the Hagen-Strunk multiplication mechanism discussed above, the breeding factor should be proportional to the number of Hagen-Strunk (HS) type intersections produced per unit length of dislocation travel. This may be expressed as

$$\delta_{HS} = \frac{p_{HS}}{2S} \qquad [30]$$

where S is the current spacing between misfit dislocations and p_{HS} is breeding efficiency, or the probability that any particular Hagen-Strunk intersection actually results in a new pair of moving dislocations. The effect of this kind of multiplication on the spacing of misfit dislocations is shown in Figure 16. Here we consider the case of a film with an initial dislocation density of N_0 =

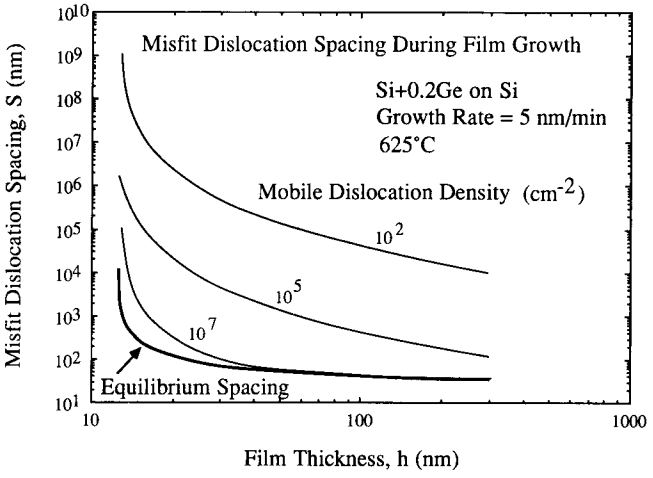

Fig. 13—Misfit dislocation spacing as a function of film thickness during growth of a Si + 0.2Ge film on a Si substrate under the conditions shown. Calculations are shown for three different threading dislocation densities. The predictions of the equilibrium theory are also shown.

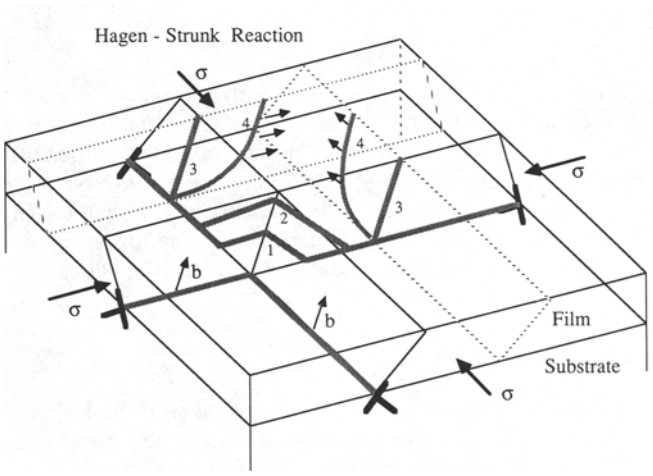

Fig. 14—Illustration of the Hagen-Strunk[22] mechanism of dislocation multiplication. Crossing dislocations with the same Burgers vectors can react to form two new mobile dislocations as shown.

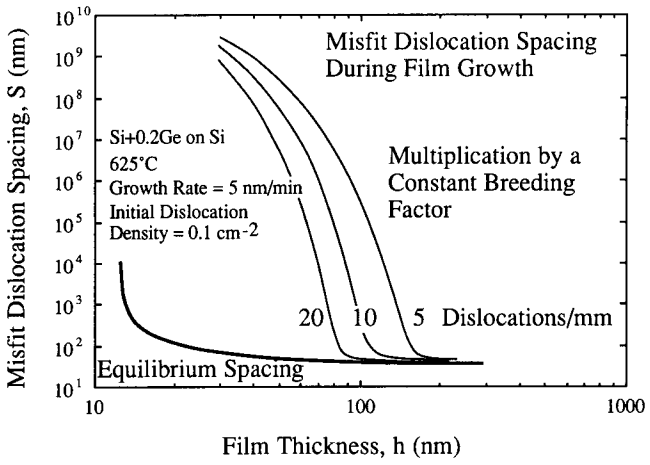

Fig. 15—Misfit dislocation spacing as a function of film thickness during growth of a Si + 0.2Ge film on a Si substrate under the conditions shown. Calculations are shown for three different rates of dislocation multiplication. The predictions of the equilibrium theory are also shown.

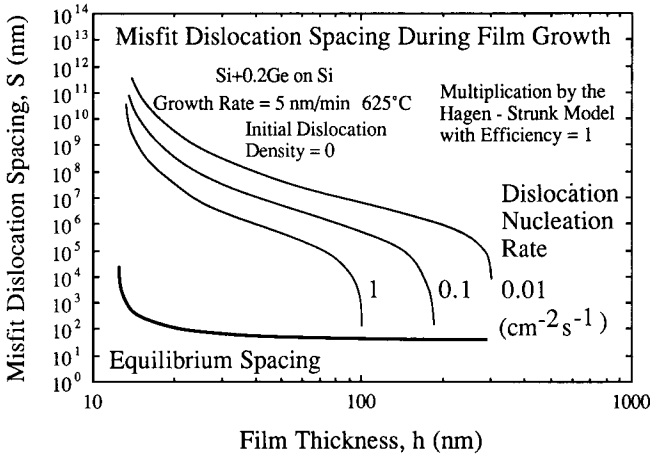

Fig. 17—Misfit dislocation spacing as a function of film thickness during growth of a Si + 0.2Ge film on a Si substrate under the conditions shown. Calculations are shown for three different rates of dislocation nucleation. The predictions of the equilibrium theory are also shown.

1000 cm^{-2}. We show the effect of Hagen-Strunk multiplication by calculating the evolution of the misfit dislocation spacing for various breeding efficiencies. The calculation involves coupling Eq. [27] with Eq. [28] and using Eqs. [29] and [30] to describe the multiplication process. We see, as expected, that multiplication can have a profound effect on the evolution of the misfit dislocation spacing. Generally, increasing the breeding factor causes the misfit dislocations to form more abruptly during film growth. Indeed, the curves of Figures 15 and 16 give the impression that the critical thickness for misfit dislocation formation is much greater than the true critical thickness of 13.5 nm. This helps to explain why misfit dislocations are often not observed in films that have been grown well beyond the critical thickness.

c. *Nucleation of dislocation half-loops*

New dislocations can also be formed by nucleation in the growing film, perhaps at the growing surface. Such nucleation must occur in those cases where misfit dislocations are formed in epitaxial films grown on dislocation-free substrates. For the present analysis, we let $(dN/dt)_0$ represent the rate of nucleation of new dislocations. Then the total rate of formation of new dislocations can be expressed as

$$\frac{dN}{dt} = \left(\frac{dN}{dt}\right)_0 + N\delta v \qquad [31]$$

When new moving dislocations are formed in the course of growth, the rate of formation of misfit dislocations is described by coupling Eq. [31] with Eq. [27]. The effect of dislocation nucleation on the evolution of the misfit dislocation spacing is shown in Figure 17 for various rates of nucleation. We see that increasing the rate of nucleation causes the misfit dislocation spacing to approach the equilibrium spacing more quickly. Nucleation of dislocations during the course of film growth makes the misfit dislocations form even more abruptly than when only multiplication effects are included in the analysis.

Note that stress relaxation during the course of film growth has been taken into account in all of the above calculations. The creation of misfit dislocations is equivalent to plastic deformation in the film and relieves the elastic strain and stress in the film. The corresponding evolution of the stress is described by

$$\frac{d\sigma}{dt} = -\frac{MNb}{2}v \qquad [32]$$

where M is the biaxial elastic modulus of the film.

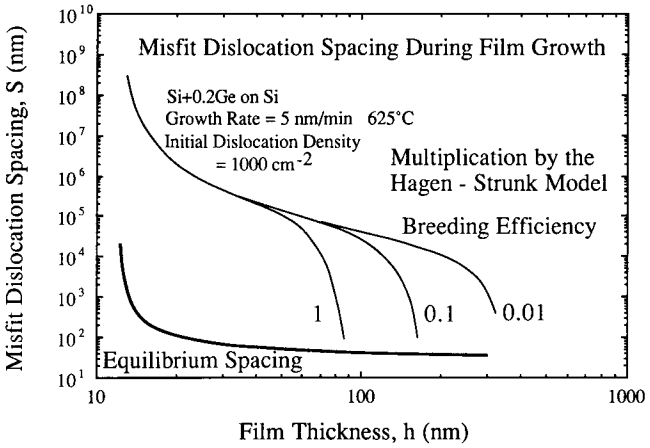

Fig. 16—Misfit dislocation spacing as a function of film thickness during growth of a Si + 0.2Ge film on a Si substrate under the conditions shown. Calculations are shown for the Hagen-Strunk multiplication mechanism with three different efficiencies. The predictions of the equilibrium theory are also shown.

VI. BIAXIAL STRENGTHS OF THIN FILMS ON SUBSTRATES

We now turn our attention to the strengths of thin films on substrates. We will see that the basic processes of misfit dislocation formation discussed above can also be used to understand plastic deformation of thin films on substrates. In addition, the relations we have developed for misfit dislocations can be used to describe the high strengths of these thin film materials.

Yielding and plastic flow in a thin film are, of course, driven by the stresses present in the film. Thus, any experimental study of biaxial strength must start with a measurement of the stress in the film. As in the case of bulk materials, the onset of plastic flow, or yielding, occurs when increments in the stress lead to nonelastic strain increments in the film. First, however, we must address the problem of measuring stress in the film.

A. *Techniques for Measuring Thin Film Stresses*

The experimental techniques for measuring stresses in thin films on substrates fall into two general classes: (1) those based on direct measurements of the elastic strains in the films using X-rays and (2) those based on the associated curvature or deflection of the substrate. The direct X-ray techniques are most informative because they permit a measurement of all of the components of stress in the film. They can, in principle, be used to detect spatial variations of stress within the film, either from grain to grain or from one point in the film to another. They can also be used to find the stresses in patterned films with irregular geometries. However, because these techniques are based on diffraction, they are limited to crystalline films; they cannot be used to find the stresses in noncrystalline materials, such as passivation glasses or amorphous oxides. For these cases, the stresses must be determined by measuring the curvature or deflection of the substrate. Even for crystalline films, the substrate curvature technique is often preferable because it is more convenient to use and easier to apply to special conditions. Such conditions include *in situ* heating or cooling or stress measurements during the course of film growth.

We saw in Section IV that the biaxial stress in a thin film on a much thicker substrate is directly proportional to the associated curvature of the substrate, provided the substrate deforms elastically. For the usual case of a substrate that is elastically isotropic in the plane of the film, the expression for the biaxial stress in the film is

$$\sigma_f = M_s \frac{h_s^2}{6h_f} K = M_s \frac{h_s^2}{6h_f} \frac{1}{R} \qquad [33]$$

where $K = 1/R$ is the curvature of the substrate, M_s is the biaxial modulus of the substrate, and h_f and h_s are the thicknesses of the film and substrate, respectively. We see that the film stress does not depend on the properties or behavior of the film. This relation is valid for both elastic and plastic deformation in the film. In most cases, the bare substrate is not perfectly flat so that the curvature, K, in Eq. [33] must be replaced by the change in curvature associated with the presence of the film. Thus, the stress in a film is found by measuring the curvature of the substrate both before and after the film is deposited or, equivalently, before and after the film is removed from the substrate.

1. *X-ray diffraction*

A variety of techniques can be used to measure the curvature changes associated with thin film stresses. For the case of single-crystal substrates, the curvature of the substrate produces a curvature of the crystal lattice that can be detected by X-ray diffraction. An advantage of this technique is that for a single film, the technique is absolute. In such a case, it is not necessary to measure the curvature before the film is deposited or after the film is removed from the substrate, because it is known that for most good substrates, such as silicon, the crystal lattice would have no curvature in either case.

2. *Optical interferometry*

Optical interferometry represents another method for measuring changes in substrate curvature. A simple count of interference fringes permits a determination of the curvature. This technique is preferable if a more general measurement facility is not available and if the induced curvature is quite large. The principle of interferometry could be used to create a rapid, quantitative stress measuring technique comparable with the laser scanning technique described below, but, as yet, such instruments are not available.

3. *Laser scanning*

The laser scanning technique is the most popular technique for measuring curvature changes associated with thin film stresses. The principle of the technique is quite simple. A beam of laser light reflects off the surface of a curved substrate at an angle θ that depends on the orientation of the surface. Upon moving (or scanning) the laser beam to a new position, the light reflects at a different angle if the substrate is curved. A position-sensitive photodetector can be used to detect the change in angle of the reflected laser beam. Flinn *et al.*[24] have recently developed a laser scanning device that makes use of a rotating mirror to scan the laser beam over the substrate. A schematic diagram of their instrument is shown in Figure 18. A lens is used to cause the rotating laser beam to be perpendicular to the substrate at all points in the scan, and the same lens causes the reflected beams to converge to one point on the position-sensitive photodetector if the substrate is perfectly flat. When the substrate is curved, the reflected beam moves to different positions on the photodetector as the laser beam is scanned across the substrate. The linear motion detected by the photodetector can be converted to changes in angle as a function of position on the substrate, and this, in turn, can be used to find the curvature of the substrate.

The laser scanning device is very sensitive and is capable of detecting the bending of a flat wafer to a radius of about 10 km. For typical film dimensions, this corresponds to a film stress of about 0.2 MPa. This sensitivity is required because the film, being so much thinner than the substrate, bends the substrate only very slightly. As noted above, bare substrates are usually not perfectly flat. They often take the form of a potato chip, although typical substrates are, of course, much flatter than potato chips. For such a shape, the curvature varies from point to point on the substrate and depends on the path of the scan. The shape of the substrate along a particular laser scan path must be found before the film is deposited or after the film is removed in order to obtain the change in curvature associated with the presence of the film. Even though the curvature of a substrate is not constant with position along the scan, the change in curvature associated with the film is often quite constant, provided that the thickness of the film is constant and the deposition conditions are the same at all points on the substrate. In such cases, the subtraction technique described

Fig. 18—Schematic diagram of a laser scanning instrument used to measure substrate curvature and associated film stress.[24]

above gives a single value for the change in curvature, and this, in turn, leads to a single value for the average biaxial stress in the film.

Throughout this discussion, we have assumed that the biaxial stress in the film does not vary through the thickness of the film. If the stress varies through the film thickness, the substrate curvature technique gives only the average value of the stress. Doerner and Brennan[25] have recently used a grazing incidence X-ray scattering (GIXS) technique to measure the biaxial stresses in films of aluminum on silicon as a function of distance from the film-substrate interface. Some of their results are shown in Figure 19. The samples were initially heated to 450 °C and allowed to relax to a stress-free state before cooling to room temperature where the measurements were made. On cooling to room temperature, much of the differential thermal strain is accommodated by plastic deformation, leaving a small residual elastic strain in the film. The X-ray technique gives the remaining elastic strain (or stress) as a function of distance from the film-substrate interface. Except for a sharp variation very near the surface of the film, the elastic strain (and stress) remains relatively constant through the thickness of the film. Thus, for this case, the substrate curvature technique can be used to determine the local biaxial stress through most of the thickness of the film. This assumption is probably not valid for films in their as-deposited state because their structure (and stress) may vary significantly through the thickness of the film.

B. *Measurement of Elastic and Plastic Deformation in Thin Films on Substrates*

In order to study the deformation properties of a thin film on a substrate, it is necessary to be able to vary the stress (or strain) and measure the corresponding changes in strain (or stress) in the film. Because the film is usually quite thin and because it is attached to the substrate,

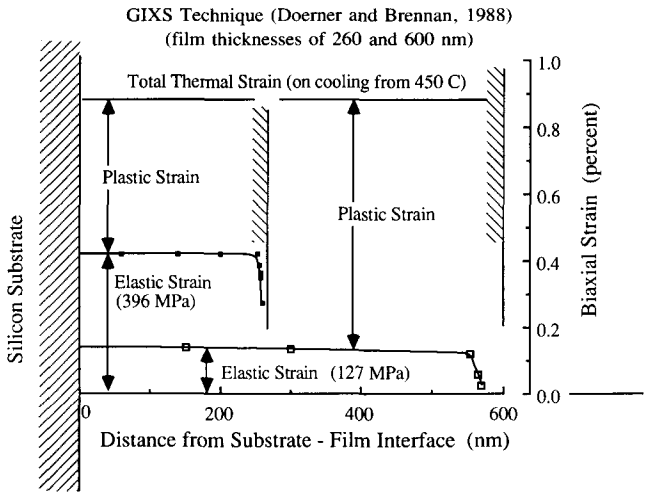

Fig. 19—Elastic strain distribution in Al films on Si substrates obtained using the GIXS technique.[25] The strains (and stresses) are uniform over most of the film thickness.

ordinary bulk mechanical testing methods cannot be used. However, we can use thermal expansion and the substrate curvature method to create a thin film mechanical testing technique. We can make use of differences in thermal expansion coefficients between the film and the substrate to impose varying biaxial strains in the film through heating and cooling. The curvature technique can then be used to measure any corresponding changes in film stress.

The results of such a testing procedure are shown in Figure 20 for the case of a polycrystalline film of aluminum on an oxidized silicon wafer. Here the substrate curvature method was used to determine the biaxial stress in the film as a function of temperature during one of several heating and cooling cycles. The film had been annealed at 450 °C prior to conducting the experiment in an effort to stabilize the grain structure. This annealing step eliminates the fine-grained microstructure found in the as-deposited state and removes special features of the stress-temperature history that occur only during the first heating cycle. It also leaves the film in a state of biaxial tension at room temperature. As shown in Figure 20, the biaxial tensile stress in the film at room temperature is about 280 MPa at the beginning of the second heating cycle. As the film-substrate composite is heated, the greater thermal expansion of the aluminum film first relaxes the tensile stress in the film and later causes the film to go into a state of compression. During the initial unloading portion of the curve, the differences in thermal expansion between the film and substrate are accommodated by elastic deformation of the film. The slope of the curve in this regime is simply the product of the difference in thermal expansion coefficients and the biaxial elastic modulus of the film, as shown in the figure. Eventually, biaxial yielding of the film in compression is observed as a deviation from the thermoelastic loading line. For a more precise definition, the biaxial yield stress would have to be determined using a suitable plastic offset, such as 0.2 pct. With continued heating after yielding, the compressive stress rises only slowly and eventually passes through a maximum. In this part of the experiment, the changing thermal strain is accommodated by compressive plastic deformation in the film. The decreasing compressive stress with increasing temperature is an indication of the expected temperature dependence of the flow stress. On cooling from 450 °C, the compressive stress is first relaxed to zero as the film thermally contracts more than the substrate. On further cooling, a tensile stress develops in the film, and this causes plastic deformation in tension to occur. The stress-temperature curve does not go through a maximum on cooling because the flow strength increases with decreasing temperature. The curve in this part of the experiment corresponds to the flow stress of aluminum as a function of temperature. Note that the stress in the film after the thermal cycle is complete is about the same as the stress at the start of the cycle. This is not unique to this particular experiment; it is commonly observed for metal films on silicon. In fact, repeated heating and cooling cycles, such as the one described here, result in stress-temperature plots that are almost identical to the one shown in Figure 20.

The stress-temperature history for an alloy of Al + 2 pct Cu that had also been annealed once prior to testing is shown in Figure 21.[26] The main features of the curve are the same as those for pure aluminum. In this case, however, the microstructure changes with temperature as the copper dissolves on heating and precipitates from solution on cooling. The effect of precipitation from solution on cooling is indicated by the rapid strengthening that occurs near 150 °C. Below that temperature, the film does not deform plastically, indicating that the yield strength exceeds the actual stress in the film.

This technique for studying the plastic deformation properties of thin films on substrates permits one to study both yielding and plastic flow. Even time-dependent plastic flow can be studied by holding the temperature constant and measuring the kinetics of stress relaxation. However, it should be noted that because the strains are thermally imposed, generally it is not possible to conduct an isothermal stress-strain deformation experiment. Thus, the stress-temperature diagrams shown in Figures 20 and 21 represent nonisothermal mechanical hysteresis curves.

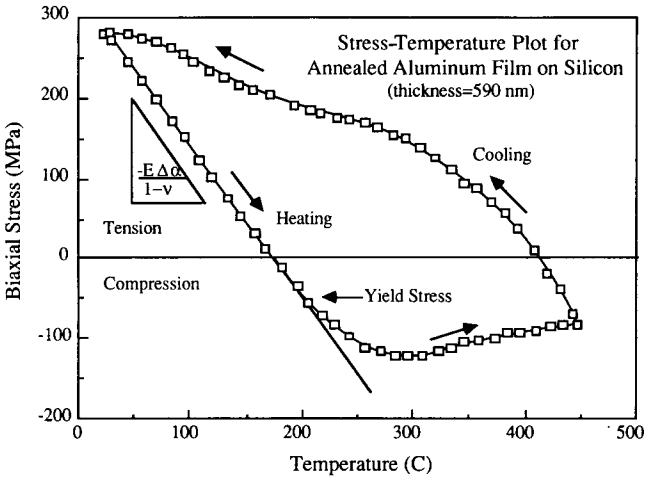

Fig. 20—Stress-temperature plot for an Al film on a Si substrate. Elastic and plastic deformation occur in the film during heating and cooling.

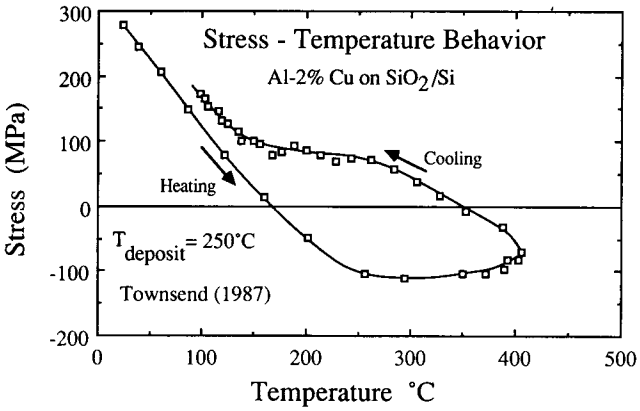

Fig. 21—Stress-temperature plot for an Al + 2 pct Cu film on a Si substrate.[26]

C. *Microstructural Changes in Thin Films*

In the examples cited above, the stress-temperature relations are dominated by the effects of elastic and plastic deformation. Any microstructural changes that occur during heating and cooling are assumed to influence the resulting stress-temperature curve only by their effects on the elastic and plastic properties. When major microstructural changes occur, this assumption is no longer valid, and the dilatational effects of microstructural changes must be included in the interpretation of the stress-temperature curve.

As noted above, the stress-temperature history for the first heating of an as-deposited film is usually quite different from the curves discussed above. An example is shown in Figure 22.[27] This film is in biaxial tension in the as-deposited state. Upon heating, the greater thermal expansion of the film compared to the substrate causes the stress to become compressive. With continued heating, the compressive stress in the film reaches a very large value before decreasing rapidly in the temperature range of 225 °C to 275 °C. This stress relaxation is not caused by plastic deformation in the film. It is the result of the densification of the film that accompanies grain growth. In the as-deposited state, the grain size in the film is extremely fine. This as-deposited grain structure is unstable; the grains begin to grow at about 225 °C and continue to grow during heating until they are comparable in size to the thickness of the film. This causes a huge stress relaxation to occur. The excess volume associated with the large number of grain boundaries in the as-deposited state is removed during heating, and this densification relaxes the compressive stress in the film. This mechanism of stress relaxation does not involve plastic deformation of the film; it is the result of a structural transformation within the film. The stress relaxation associated with grain growth occurs only during the first heating cycle. For subsequent heating and cooling cycles, the grain structure remains essentially constant, and the stress-temperature curves are dominated by elastic and plastic deformation of the film. The stress changes associated with grain growth could cause the stress to change sign. If the tensile stress in the as-deposited state was greater, then grain growth would have caused the stress to go back into tension in the temperature range of 250 °C to 300 °C.

In some cases, the stress-temperature relations are almost completely dominated by structural transformations that occur upon heating and cooling. An example is shown in Figure 23 for a chemically vapor-deposited (CVD) film of WSi_2 on Si.[26] This film is essentially amorphous in the as-deposited state and is in a state of biaxial tension. The stress decreases slightly on heating due to the differences in thermal expansion of the film and substrate. At about 500 °C, the film crystallizes and densifies, causing the tensile stress in the film to increase abruptly. At still higher temperatures, the film begins to deform plastically, and this causes the stress to relax. Heating to 900 °C leads to a very stable microstructure that does not change during subsequent heating and cooling cycles. After the structure has been stabilized in this way, the film deforms in a purely reversible, elastic manner on subsequent heating and cooling.

D. *Strengths of Thin Films on Substrates*

We now consider the mechanisms of plastic deformation in thin films on substrates. We wish to understand the factors that control the strengths of these thin film materials. We note that materials in thin film form exhibit much higher strengths than their bulk counterparts. For example, the data in Figure 20 indicate that the room-temperature yield strength of pure aluminum is about 280 MPa in thin film form. The compressive flow stress at high temperatures is about 100 MPa. These strengths are much higher than those found for bulk pure aluminum.

The high strengths of thin films on substrates can be attributed partly to the fine microstructures found in these materials. As noted above, even after annealing, the grain

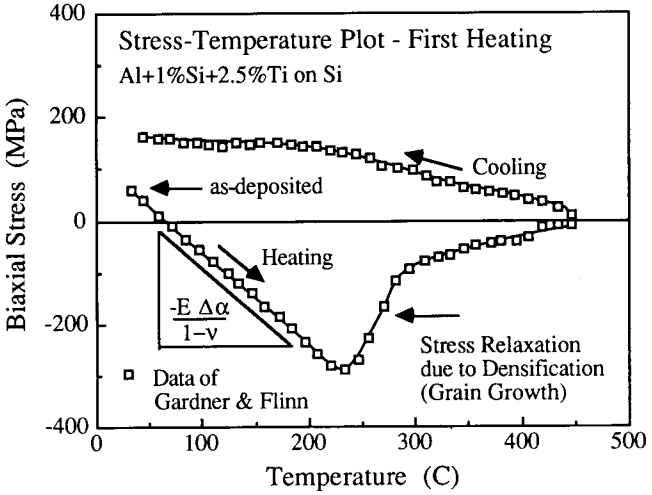

Fig. 22—Stress-temperature plot for an Al + 1 pct Si + 2.5 pct Ti film on a Si substrate.[27] The stresses observed during the first heating and cooling cycle are shown. The large stress relaxation observed near 250 °C is caused by densification of the film *via* grain growth.

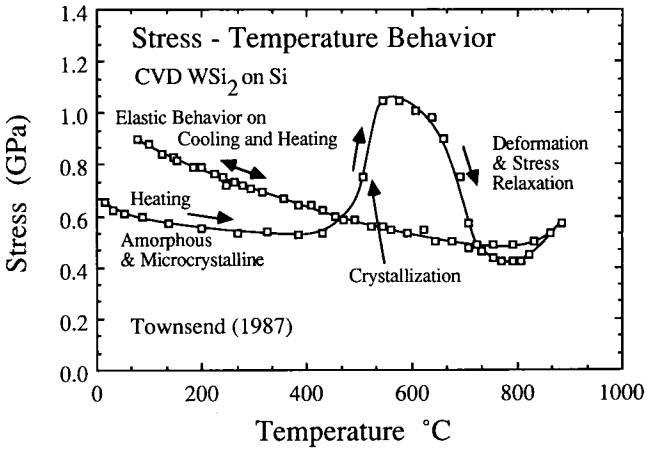

Fig. 23—Stress-temperature behavior for an initially amorphous film of CVD WSi_2 on a Si substrate. The large peak is caused by crystallization and deformation of the film. A purely elastic response is observed for subsequent heating and cooling cycles.

size typically does not exceed the thickness of the film. As a consequence, significant grain size strengthening occurs naturally in these thin film materials. In addition, the dislocation densities in thin films can be quite high, and this also contributes to the high strengths of these materials. However, these microstructural factors cannot fully account for the high strengths of thin films on substrates. Much of the strength can be attributed to the fact that the substrate constrains dislocation motion in the film. Any oxides that may be present on the surface of the film can also constrain the movements of dislocations within the film. The effects of these constraints on dislocation motion are shown in Figure 24. Here we envision a single-crystal film attached to a substrate; the film is assumed to have a nondeformable oxide on its surface. A single dislocation moving within the film must leave a dislocation line at each interface as it moves. In this respect, the dislocation motion is analogous to the movement of threading dislocations in epitaxial films. We can use the approach developed for threading dislocations to describe the motion of dislocations in thin films, and this will permit us to understand the high strengths of thin films on substrates.

1. *The misfit dislocation model*

Following the approach developed by Freund,[17] we consider the work done by the biaxial stress in the film when the dislocation travels a unit distance. For the geometry shown in Figure 24, this may be expressed as

$$W_{\text{layer}} = \frac{\cos\phi\cos\lambda}{\sin\phi}\sigma bh \qquad [34]$$

where σ is the biaxial stress in the film, b is the Burgers vector, and h is the thickness of the film. Here we have retained the notation of Eq. [19] and used the subscript "layer" to indicate the work done by the stress in the film. In order for the dislocation to move, the work done by the stress in the film must be equal to or greater than the energies of the two dislocations left at the film-substrate and film-oxide interfaces, which we express as

$$W_{\text{dislocations}} = \frac{b^2}{4\pi(1-\nu)}\left[\frac{2\mu_f\mu_s}{(\mu_f+\mu_s)}\ln\left(\frac{\beta_s h}{b}\right) + \frac{2\mu_f\mu_o}{(\mu_f+\mu_o)}\ln\left(\frac{\beta_o t}{b}\right)\right] \qquad [35]$$

where μ_f, μ_s, and μ_o are the elastic shear moduli of the film, substrate, and oxide, respectively, h and t are the thicknesses of the film and oxide, and $\beta_s = 2.6$ and $\beta_o = 17.5$ are numerical constants. By equating W_{layer} to $W_{\text{dislocations}}$, we obtain an expression for the minimum biaxial stress needed to move the dislocation in the film:

$$\sigma = \frac{\sin\phi}{\cos\phi\cos\lambda}\frac{b}{2\pi(1-\nu)h}\left[\frac{\mu_f\mu_s}{(\mu_f+\mu_s)}\ln\left(\frac{\beta_s h}{b}\right) + \frac{\mu_f\mu_o}{(\mu_f+\mu_o)}\ln\left(\frac{\beta_o t}{b}\right)\right] \qquad [36]$$

This is an expression for the minimum biaxial yield strength of a single-crystal thin film on a substrate. No obstacles to dislocation motion, such as other dislocations, point defects, or grain boundaries, have been assumed, and no friction stress for dislocation motion has been considered. If an oxide is not present on the surface of the film, the second term in the brackets should be deleted. The most important feature of this result is the prediction that the yield strength of the film depends inversely on the thickness of the film. This helps to explain why very thin films have high yield strengths.

2. *Comparison of the model with experiment*

The predictions of Eq. [36] can be compared with the measured strengths of thin films on substrates. Kuan and Murakami[28] have used X-ray techniques to measure the biaxial yield strengths of polycrystalline films of Pb on silicon at 4.2 K as a function of film thickness. Some of their results are shown in Figure 25. The films exhibit a strong ⟨111⟩ texture and have a large grain size. The predictions of Eq. [36] are shown as a solid line in the figure. The following constants were used in this calculation: $\mu_f = 13.6$ GPa, $\mu_s = 66.5$ GPa, $\mu_o = 64$ GPa, $b = 0.35$ nm, $\nu = 0.376$, $t = 5$ nm, and $\sin\phi/\cos\phi\cos\lambda = 3.464$. The model gives a good account of the strengths of these films. Doerner *et al.*[29] have also measured the biaxial strengths of thin films of pure aluminum as a function of film thickness using the substrate curvature technique described earlier. The stress-temperature curves for two different film thicknesses are

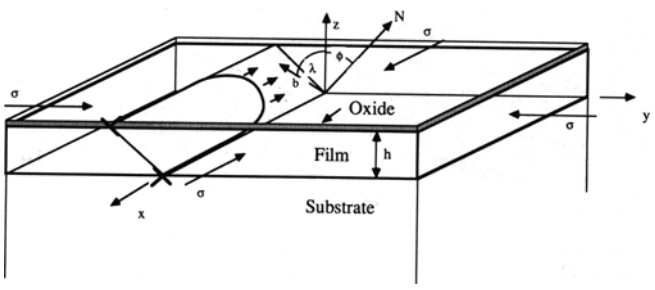

Fig. 24 — Dislocation motion in an oxidized film on a nondeformable substrate. Misfit dislocations are produced at the two interfaces.

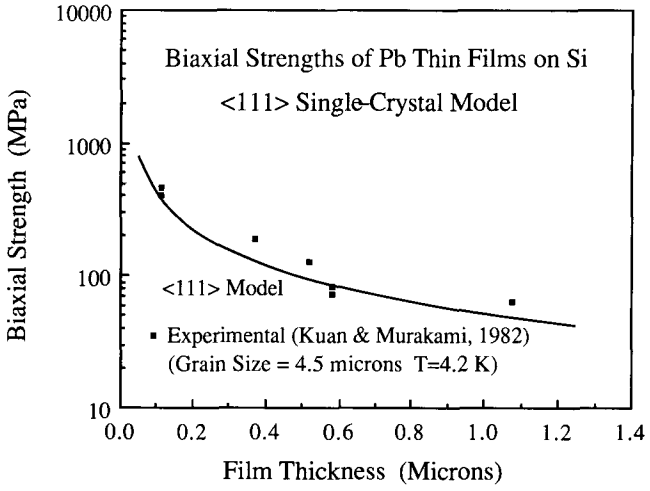

Fig. 25 — Biaxial strengths of Pb thin films on Si substrates as a function of film thickness.[28] Predictions of the misfit dislocation model for film strength are shown for comparison.

shown in Figure 26. Note that the strength of the thinner film is greater at both high and low temperatures. This suggests that an athermal strengthening mechanism is primarily responsible for the strength of the film. The mechanism described earlier is essentially athermal, as indicated by the absence of a strongly temperature-dependent term in Eq. [36]. The predictions of Eq. [36] are compared with the experimental results of Doerner *et al.*[29] in Figure 27. The curve labeled σ_o represents the prediction of Eq. [36] using the following constants: μ_f = 24.8 GPa, μ_s = 66.5 GPa, μ_o = 178.9 GPa, b = 0.286 nm, ν = 0.31, and sin ϕ/cos ϕ cos λ = 3.464. It is evident that the measured yield strengths are greater than the predictions of Eq. [36], especially at the larger film thicknesses. The discrepancy is due to the omission of grain size strengthening in the above model. Doerner[30] measured the grain sizes of the aluminum films with TEM and found a systematic variation of grain size with film thickness. She found the grain size to be about $1.3h$, where h is the thickness of the film. Using this relation together with the Hall-Petch coefficient of $k_y = 6 \times 10^4$ N/m$^{3/2}$ reported for bulk aluminum by Hansen[31] and Armstrong,[32] we can find the grain size contribution to the strength. This contribution is shown as a solid line labeled $k_y d^{-1/2}$ in Figure 27. By adding this contribution to σ_o, we obtain a prediction that is in reasonable agreement with the data. A grain size contribution is negligible for the Pb data of Figure 25 because the grain size is so much larger than the film thickness.

We have argued that the constraint of the substrate makes a significant contribution to the strength of a thin film on a substrate. One way to check this prediction is to compare the strengths of thin films on substrates with the strengths of free-standing thin films. A comparison of this kind is shown in Figure 28. Here the yield strength data of Doerner *et al.*[29] for pure aluminum films on silicon are compared with biaxial yield strengths of free-standing thin films of Al + 1 pct Si reported by Griffin *et al.*[33,34] Griffin's data were obtained by bulge testing of free-standing films, so they do not include the effect of the constraint of the substrate. All of the data are plotted according to the Hall-Petch relation. The data of Griffin *et al.*[33,34] were obtained for films with a constant thickness of 1 μm, whereas the data of Doerner *et al.*[29] were obtained for films of various thicknesses. Thus, the Hall-Petch slope for the Doerner data is somewhat misleading because much of the strengthening is actually caused by the constraint of the substrate. The Hall-Petch slope for bulk polycrystalline aluminum is shown for comparison. We note that the strengths of the aluminum films bonded to the silicon substrate are much greater than the strengths of the free-standing films. The constraining effect of the substrate makes these films even stronger than bulk aluminum of comparable grain size. These comparisons support the idea that much of the strength of thin films on substrates is caused by the constraint of the substrate.

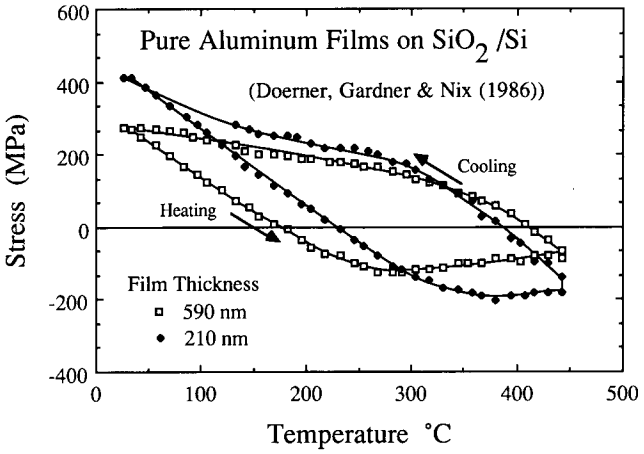

Fig. 26—Stress-temperature plots for thin films of Al on a Si substrate.[29] The results show that the thinner film is stronger than the thicker film at both low and high temperatures.

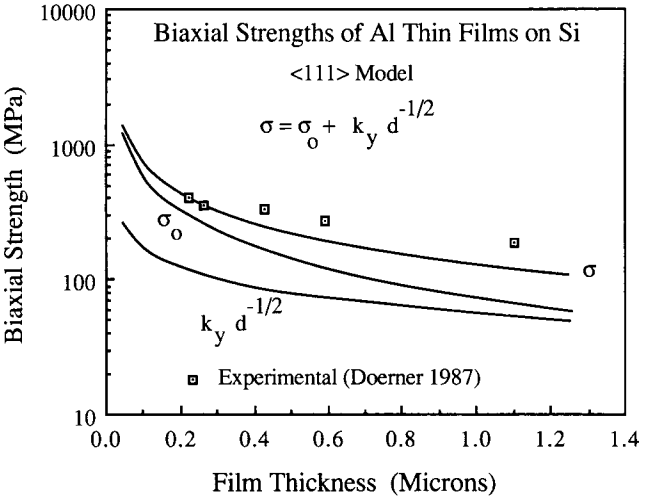

Fig. 27—Biaxial strengths of Al thin films on Si substrates.[29] The predictions of the misfit dislocation model for film strength are shown for comparison. Hall-Petch strengthening must be included to account for the high strengths of the films.

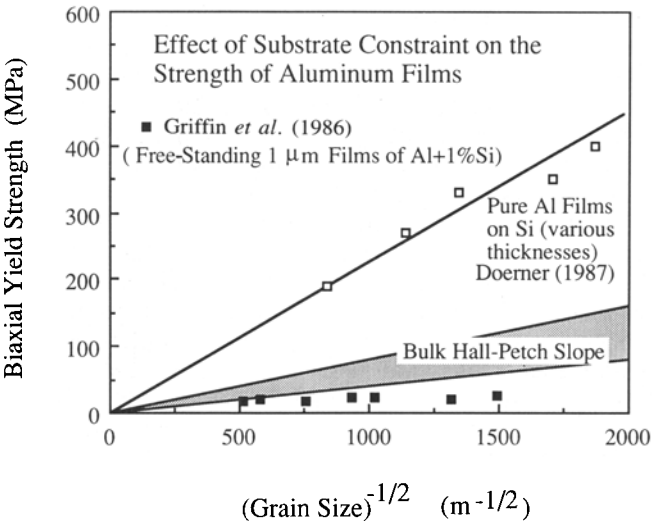

Fig. 28—Comparison of the strengths of the Al films on Si substrates[30] with the biaxial strengths of free-standing films of Al + 1 pct Si[33,34] in the form of a Hall-Petch plot. The constraint of the substrate causes the films bonded to the substrate to be much stronger than the free-standing films.

VII. SUBMICRON INDENTATION TESTING TECHNIQUES

In conventional studies of the mechanical behavior of materials, it is common practice to create test samples of the material in question, subject them to forces or displacements, and measure the corresponding response. Usually, simple stress states, such as tension, compression, and torsion, are used to permit the calculations of stress and strain from the measured forces and displacements. Such an approach cannot be used to study the mechanical properties of thin films on substrates because the thin films of interest are typically 1 μm in thickness or less and are bonded to substrates. Submicron indentation represents an alternative approach. By measuring the forces needed to create small indentations in thin films on substrates, it is possible to obtain information about the elastic and plastic properties of the film material. An inherent complication of this approach is that the stresses and strains produced by indentation are nonuniform within the test sample. Therefore, only nominal values of the stresses, strains, and strain rates can be determined in such tests. Nevertheless, submicron indentation gives some information about the mechanical properties of thin films that cannot be obtained easily in any other way.

A. *Depth-Sensing Indentation Instruments*

Although indentation hardness testing has been in widespread use for more than a century, high-resolution (submicron) indentation instruments have become available only recently. Most of the instruments that are available have been built by individual investigators to meet specific research requirements.[35–43] In the traditional approach to the determination of hardness, a fixed load is imposed on a diamond indenter, and the resulting indentation is observed. The hardness is taken to be the load divided by the projected area of the permanent indentation. This approach has been adopted by Bangert *et al.*[40] in their development of a microindentation attachment used in conjunction with a scanning electron microscope. Other instruments that do not require the direct observation of the indentation have also been developed.[35–39,41–43] These instruments are called depth-sensing because both the load on the indenter and the displacements associated with indentation are measured in the course of indentation. An instrument of this kind, called the Nanoindenter, was developed by Pethica and Oliver[37,43] and is commercially available. Stanford University has such a device, and results obtained with that machine will be presented here. The basic characteristics of this instrument and the mechanical properties that can be measured with it are described below. Other instruments of this kind have been built by other investigators. Most of these are, like the Nanoindenter, load-controlled instruments in which the force on the indenter is imposed, and the resulting displacement of the indenter into the material is measured.[35–39] These instruments can be regarded as "soft" testing machines in the sense that the load on the indenter is not changed by the penetration of the indenter into the material but rather is controlled by the loading mechanism. Such instruments are analogous to creep machines in ordinary mechanical testing. Another form of microindentation can be done under displacement control. Li and Wu and their collaborators[41,42] have developed instruments that allow the displacement of the indenter into the material to be imposed and the resulting load to be measured. Such instruments are analogous to "hard" testing machines that are typically used in tensile testing. They are also well suited for the study of stress relaxation in indentation.[41,44]

The microindentation experiments described here are characterized by the condition that the indenter makes increasing contact with the material during indentation. A different kind of mechanical response is observed when the indenter is flat-ended and has the shape of a right circular cylinder. For such an indenter, the projected contact area does not change as the indenter is pushed into the material. This response has been called impression testing by Yu *et al.*[45,46,47] and has been used to study the mechanical properties of small volumes of material. However, the impression tools used in such instruments are typically too big to be used in the study of most thin films on substrates.

B. *The Nanoindenter*

A schematic diagram of the Nanoindenter is shown in Figure 29.[37,48] A diamond indenter is fixed to the end of a loading shaft that is suspended on delicate leaf springs. The leaf springs are compliant in the loading direction but stiff in the transverse direction. When the indenter is not in contact with the material, the shaft is supported both by the suspending springs and a force that is delivered by the coil and magnet assembly at the top of the shaft. Movement of the indenter toward the sample is accomplished by reducing the force supplied by the magnet-coil assembly. The smallest load increment that can be made with the Stanford instrument is about 0.25 μN, and the maximum force that can be exerted is 120 mN. Motion of the indenter toward the sample is measured by a capacitance displacement gage with a displacement resolution of 0.4 nm. With this resolution, it is possible to make indentation measurements in materials with total indentation depths as shallow as about

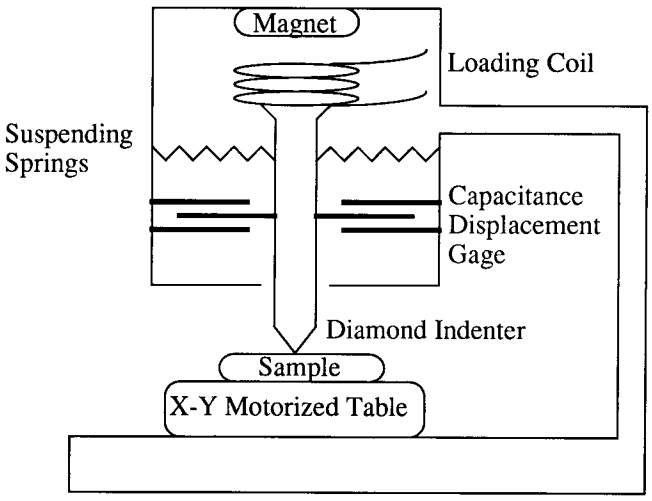

Fig. 29—Schematic diagram of the Nanoindenter.

20 nm. As noted above, the indentation made by the indenter is not observed but rather is determined from the measured depth of indentation and the known shape of the indenter. The sample is mounted on an X-Y table that allows indentations to be precisely located with respect to each other on the same surface. The position of the first indentation of an array can be placed within a few micrometers of a given location; the remaining indentations of the array can be placed with respect to the first one with a resolution of about 0.5 μm.

Indenters of any shape can be used in microindentation, but since small contact areas are needed, the best shape is the three-faced Berkovich indenter shown in Figure 30. Because any three nonparallel planes intersect at a single point, it is relatively easy to grind a sharp tip on an indenter if the three-faced Berkovich geometry is used. The angles of the faces are fixed so that the nominal relationship between the area and depth of indentation is the same as for the Vickers indenter. Invariably, the tip of the indenter is rounded so that the ideal geometry is not maintained near the tip. As shown schematically in Figure 31, the actual depth of indentation produces a larger contact area than would be expected for an indenter with an ideal shape. We use the effective depth, h_{eff}, to indicate the depth of indentation that would be needed for an ideally shaped indenter to produce the same contact area as the nonideal tip for a plastic depth, h_p. For the Berkovich (and Vickers) indenter, the nominal shape is characterized by

$$\sqrt{A} = kh_{eff} = 24.5h_{eff} \qquad [37]$$

where A is the contact area between the indenter and the material. For the diamond indenter used in most of the Stanford tests, the radius of curvature at the tip is about 300 nm.

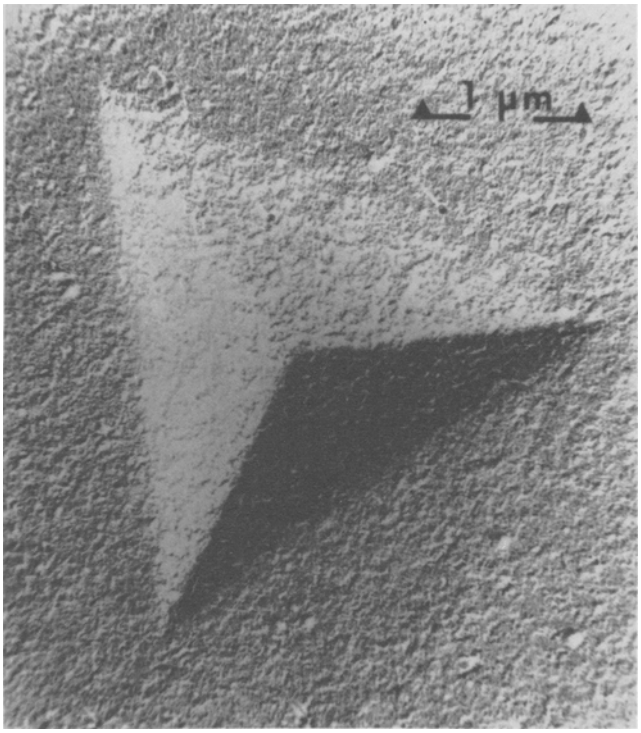

Fig. 30—Replica TEM micrograph of the Berkovich indentation.

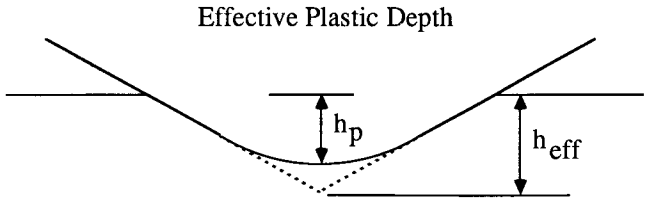

Fig. 31—Definitions of the plastic depth and the effective depth for an indenter with a nonideal shape. The effective depth is the depth at which an ideal indenter would create the same contact area as the real indenter.

C. *Indentation Mechanical Properties*

In a typical experiment, the tip of the indenter is moved toward the surface of the sample by gradually increasing the load on the indenter shaft. With a constant loading rate of 1 μN/s, the tip of the indenter travels downward at a velocity of about 20 nm/s. When the tip contacts the surface, its velocity drops below 1 nm/s, and the computer records the displacement of the tip. This is the point at which the indentation experiment begins. The loading rate is subsequently adjusted to maintain the descent velocity between 3 and 6 nm/s. A typical indentation loading curve is shown schematically in Figure 32, where the load on the indenter is plotted against the depth of indentation. The process of indentation causes both elastic and plastic deformation to occur, as shown in Figure 33. The tip of the indenter is usually sharp enough to cause plastic flow to occur from the very beginning of the test so that an elastic-plastic transition typical of an ordinary tensile test is not observed. The slope of the loading curve increases with depth of indentation because the indenter makes increasing contact with the material during indentation. The hardness of the material can be found by dividing the indentation force by the contact area at each point along the loading curve. This permits a measurement of the hardness as a function of the indentation depth. If the load is held constant, the indenter will continue to sink into the material in a time-dependent manner as creep flow under the indenter occurs. This allows a study of the creep properties of very

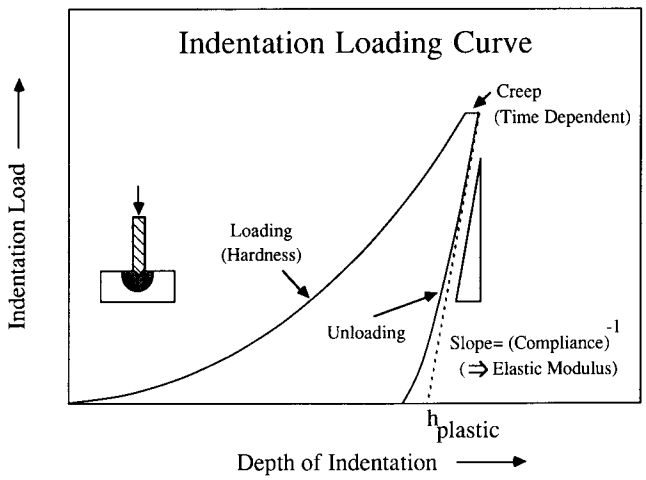

Fig. 32—Indentation loading and unloading curves. Hardness, creep, and elastic properties can be obtained from these data.

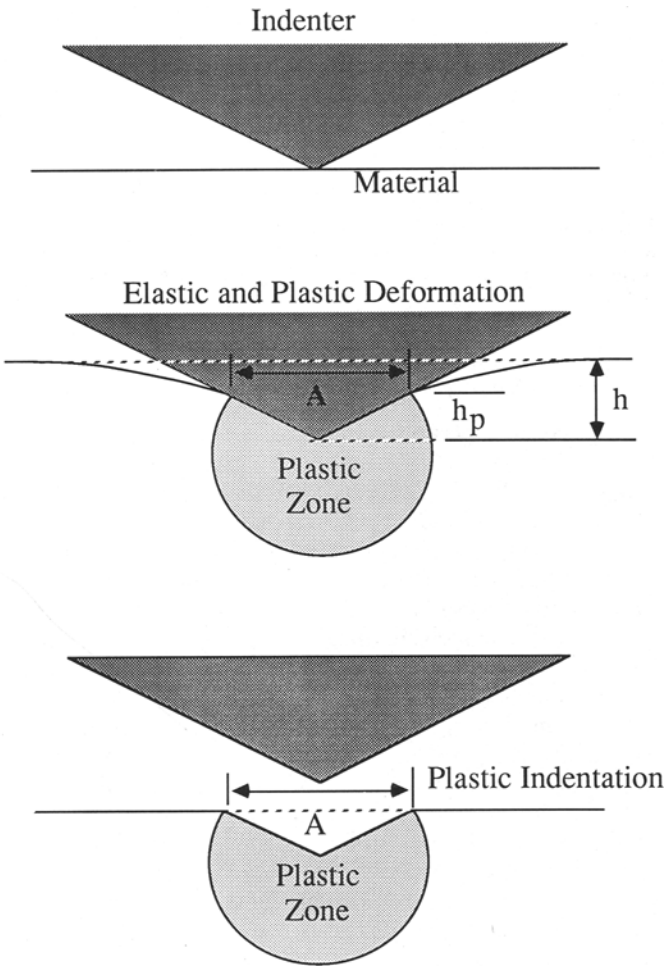

Fig. 33—Illustration of elastic and plastic deformation associated with indentation.

small volumes of material. During unloading, the indenter is pushed back out of the material by the elastic restoring forces in the system. This effect can be used to determine elastic properties. We begin our discussion of mechanical properties by showing that the elastic properties of materials can be determined by analyzing the unloading portion of the indentation curve.

1. *Elastic properties*

From the slope of the unloading curve, it is possible to determine the elastic modulus of the material being indented, provided the contact area and the elastic properties of the indenter are known. Loubet *et al.*[38] showed that the slope of the unloading curve could be modeled by treating the indenter as a flat-ended elastic punch causing displacements to occur in an elastic half-space. According to such a model, the unloading slope is given by

$$\frac{dP}{dh} = \beta E^* \sqrt{A} \qquad [38]$$

where P is the load, h is the depth of indentation, A is the contact area, β is a constant that depends slightly on the shape of the indenter, and E^* is an effective modulus for the system defined by

$$\frac{1}{E^*} = \frac{1 - \nu_0^2}{E_0} + \frac{1 - \nu^2}{E} \qquad [39]$$

where E_0 and ν_0 are Young's modulus and Poisson's ratio of the indenter, respectively, and E and ν are the same elastic properties of the material being indented. For a cylindrical punch, Sneddon[49] showed that the constant β is $2/\pi^{1/2}$. King[50] later showed that the constant is only slightly different for other shapes:

$$\text{Circle} \quad \frac{\sqrt{\pi}}{2}\beta = 1.0$$

$$\text{Square} \quad \frac{\sqrt{\pi}}{2}\beta = 1.011$$

$$\text{Triangle} \quad \frac{\sqrt{\pi}}{2}\beta = 1.034$$

The nonlinearity of the unloading curve indicates that the contact area decreases during the course of unloading. In order to determine the contact area at the point of maximum load, the slope of the unloading curve is extrapolated to zero load and the abscissa is read as the plastic depth, as shown in Figure 32. The plastic depth measured in this way, together with a knowledge of the shape of the indenter obtained from calibration experiments, permits a determination of the contact area. This contact area is related to the effective depth, h_{eff}, using Eq. [37]. Because the compliance of the Nanoindenter itself contributes to measured displacements at high loads, it is preferable to write Eq. [38] in terms of the compliance:

$$\frac{dh}{dP} = C_m + C_{\text{indent}}$$
$$\frac{dh}{dP} = C_m + \frac{1}{\beta\sqrt{A}}\frac{1}{E^*} \qquad [40]$$

where C_m is the compliance of the machine and C_{indent} is the compliance of the indenter and material. Using Eq. [37], this expression can be written in terms of the effective depth, h_{eff}, as

$$\frac{dh}{dP} = C_m + \frac{1}{\beta k}\frac{1}{E^*}\frac{1}{h_{\text{eff}}} \qquad [41]$$

We see that the measured compliance should vary linearly with the reciprocal of the effective indentation depth. As shown schematically in Figure 34, the slope of a plot of compliance *vs* the reciprocal of the effective depth gives a measure of the effective modulus of the system. The elastic properties of materials can be measured in this way. Some results for various materials are given in Figure 35 and compared with elastic constants taken from the literature. The agreement is very good for soft materials, such as aluminum. For harder materials, the indentation experiments give moduli that are higher than expected. We believe this is caused partly by the high pressure under the indenter. Some densification of SiO_2 may occur under the indenter, and this may cause an increase in the elastic modulus. The pressure can also

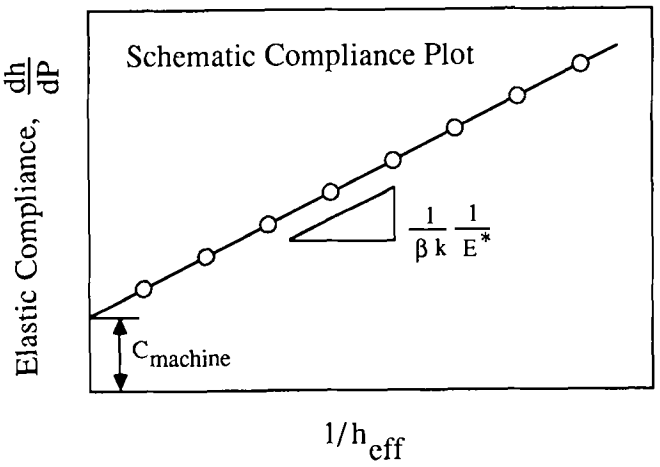

Fig. 34—Schematic plot of the elastic compliance as a function of the reciprocal of the effective depth for an indentation system. The intercept gives the elastic compliance of the machine and the slope permits a calculation of the elastic properties of the material being indented.

increase the elastic modulus of the material just under the indenter through nonlinear elastic effects. This may contribute to the higher values of elastic modulus found for silicon and tungsten.

It should be noted that the procedure outlined here for the measurement of elastic properties can be applied to hard materials that show little or no plastic indentation. In the limit of no plastic deformation (with no friction), the unloading curve would coincide exactly with the loading curve, and all of the displacements associated with indentation would be elastic. Under these limiting conditions, the slope of the curve at any point would indicate the contact area at that point. Pethica and Oliver[43] showed that purely elastic deformation is observed for

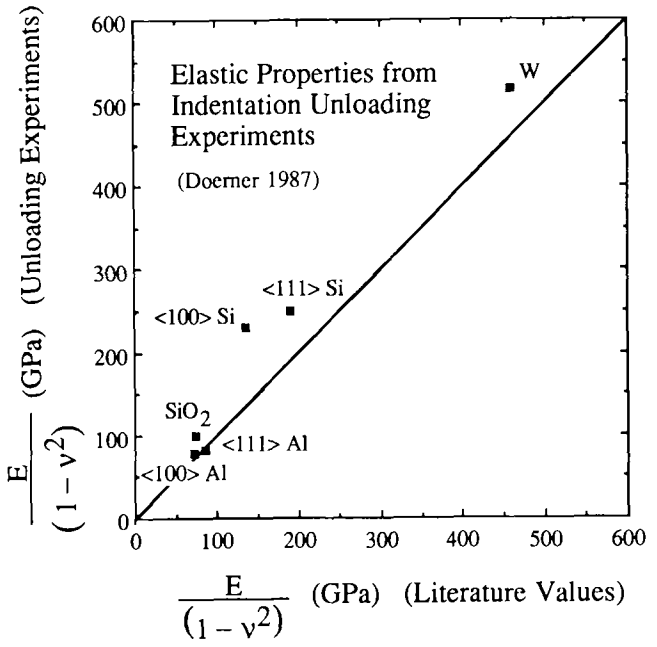

Fig. 35—Elastic properties of several materials obtained by indentation unloading experiments.[48] The results are compared with literature values of the elastic properties. The agreement is best for soft metals such as Al.

small indentations in electropolished single crystals of tungsten. They assumed that for small indentations, the contact pressures are insufficient to cause dislocation nucleation and motion to occur in tungsten. They found the elastic properties to be well described by Eq. [38] in this regime. They also showed that for larger indentations, plastic flow occurs as a sudden increase in indenter displacement at a critical contact pressure. This event is assumed to coincide with the nucleation of dislocations under the indenter. That a critical contact pressure is needed for dislocation nucleation had been confirmed in earlier work on sapphire by Page *et al.*[51]

The elastic properties of thin films on substrates can also be measured by indentation.[48,50,52] It is evident that the indentation compliance should depend on the depth of indentation compared to the thickness of the film. It is expected that for very large indentations, the compliance should be dominated by the elastic properties of the substrate, whereas for small indentations, the compliance should be dominated by the elastic properties of the film. Doerner and Nix[48] proposed a simple phenomenological relation to describe the relative contributions of the film and substrate to the indentation compliance. Their expression for the indentation compliance (after subtracting the machine compliance from the measured compliance) is

$$\left(\frac{dh}{dP}\right)t = \frac{1}{\beta k}\left(\frac{t}{h_{\text{eff}}}\right)\left\{\frac{1-\nu_0^2}{E_0} + \frac{1-\nu_s^2}{E_s}\exp\left(-\frac{\alpha}{k}\frac{t}{h_{\text{eff}}}\right) + \frac{1-\nu_f^2}{E_f}\left[1-\exp\left(-\frac{\alpha}{k}\frac{t}{h_{\text{eff}}}\right)\right]\right\} \quad [42]$$

where E_s and ν_s stand for the elastic properties of the substrate, E_f and ν_f stand for the elastic properties of the film, t is the film thickness, and α is a parameter that characterizes the transition from film to substrate control. The expression shows that the product of the compliance and the film thickness depends uniquely on the ratio of the film thickness to the effective depth. Doerner and Nix[48] showed that this relation could be used to describe the elastic properties of thin films of tungsten on silicon if α was chosen to be 1.24. Their results are shown in Figure 36. The solid lines indicate the compliances of bulk silicon and tungsten. For small values of t/h_{eff} (*i.e.*, large indentation depths), the compliance data coincide with the compliance of the silicon substrate, as expected. For large values of t/h_{eff} (*i.e.*, small indentation depths), the compliance data approach the compliance of bulk tungsten. Thus, the experiment shows how it might be possible to determine the elastic properties of thin films on substrates from the composite modulus of the film and substrate.

Recent theoretical work by King[50] has confirmed that Eq. [42] gives a good account of the indentation elastic properties of thin films on substrates. However, King's work indicates that the parameter α is not constant but varies slightly with the relative depth of indentation.

2. *Hardness*

As noted earlier, hardness is usually defined as the load divided by the projected area of the indentation left

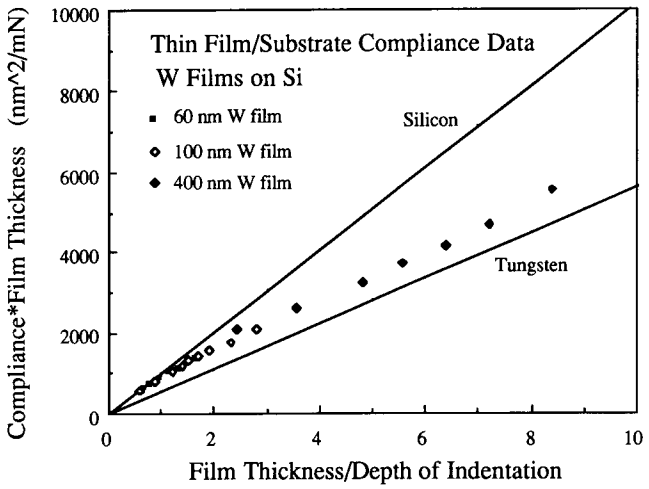

Fig. 36—Elastic properties of thin films of W on Si substrates as determined from the measurement of unloading compliances.[48] The solid lines which indicate the measured compliances of bulk W and Si also represent the limiting compliances for the thin film/substrate measurements.

by the indenter. The problem of measuring the hardness of thin films on substrates is to avoid the influence of the substrate in the measurement. For the case of metal films on silicon, the substrate is typically much harder than the film. In this case, the indentation used to make the hardness measurement must be small compared to the film thickness. The displacement resolution of the Nanoindenter permits measurements of this kind to be made.

Hardness measurements for a pure aluminum film, 1 μm thick, deposited onto an oxidized silicon substrate are shown in Figure 37 as a function of the depth of indentation. The smallest indentations give hardnesses that coincide with the hardness of single-crystal aluminum. This is to be expected, as the smallest indentations probably occur within a single grain of aluminum. The measured hardness increases slightly with the depth of indentation, as expected. The harder substrate causes the measured hardness to increase when the plastic zone under the indenter reaches the film-substrate interface. An elastic-plastic finite-element analysis of this indentation problem has been made by Bhattacharya and Nix.[52] One of their results is shown in Figure 37. This continuum analysis shows that the hardness should increase gradually with increasing depth of indentation, especially for indentation depths greater than about 20 pct of the thickness of the film. The calculated hardness does not reach the substrate hardness even for large indentation depths because most of the indenter still rests on the soft aluminum film.

The good agreement between the finite-element analysis and the measured hardness does not extend to thinner films. As shown in Figure 38, for thinner films, the measured hardness increases much more abruptly with indentation depth than the finite-element analysis predicts. Several factors are believed to be responsible for this effect. The thinner films are known to have much finer grain sizes, so that a Hall-Petch hardening effect is to be expected. In addition, as discussed earlier in connection with misfit dislocations, dislocation motion in thin films requires higher shear stresses than in the bulk because of the constraining effect of the nondeformable substrate. This, too, may help to explain why the hardness of very thin films is so much greater than the predictions of the continuum analysis.

3. *Creep and time-dependent deformation*

Because the rate of movement of the indenter can be measured with the Nanoindenter, it is possible to study the effects of strain rate on deformation in the indentation mode. This provides an additional experimental variable in the study of thin film deformation. Here we describe the techniques that have been developed to study strain-rate effects in indentation and show results that have been obtained for bulk materials.

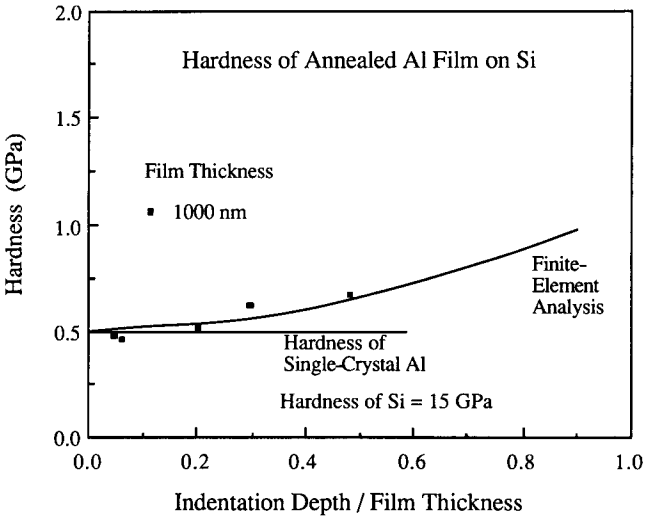

Fig. 37—Hardness of an Al film on a Si substrate as a function of the depth of indentation.[29] The results of a finite-element analysis are also shown for comparison.[52] The continuum treatment gives a good description of the data for a film of this thickness and grain size.

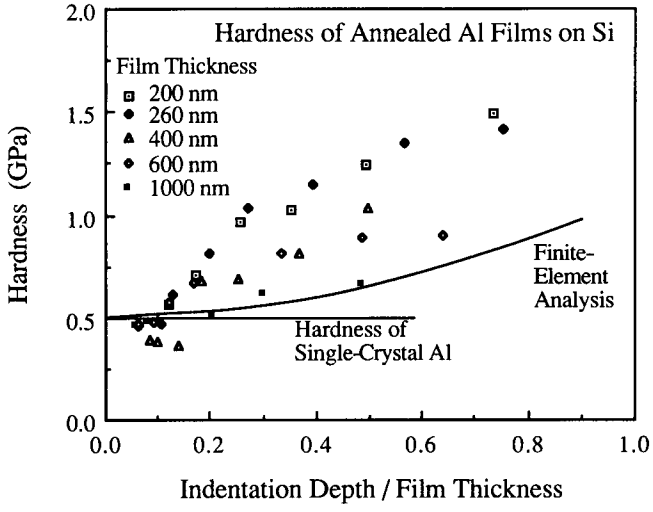

Fig. 38—Hardness of a series of Al films on Si substrates as a function of the depth of indentation.[29] The results of a finite-element analysis are also shown for comparison.[52] The continuum treatment does not give a good description of the data for the thinner films with the finer grain sizes.

As discussed above, the stresses and strains associated with indentation are nonuniform. Thus, the stress and strain-rate vary with radial distance from the point of contact. As a result, only nominal values of stress and strain rate can be calculated from the measured indentation force and velocity. As shown in Figure 39, we define the stress as the average pressure acting on the contact surface, $\sigma = P/A$, and the strain rate as the indentation velocity divided by the indentation depth, $\dot{\varepsilon} = (1/h)\ (dh/dt)$. Stresses and strain rates at any point in the sample are expected to scale with these quantities. Thus, the strain-rate sensitivity can be found using these nominal quantities.

For soft metals and alloys, the elastic displacements associated with indentation are usually small so that the total depth of indentation can be taken to be the plastic depth. For this reason, the nominal strain rate can be calculated from the indentation velocity and the total depth at that point in the indentation. A complication does arise, however, for soft metals that exhibit strain hardening. The measured hardness of these materials typically decreases with depth of indentation. This may be caused, in part, by the fact that the "geometrically necessary" dislocation density decreases with increasing indentation size. A simple argument reveals that the geometrically necessary dislocation density varies reciprocally with the depth of indentation, and this can be used to explain the depth dependence of the hardness. Because of these effects, the relationship between stress and strain rate must be determined at a fixed indentation depth to avoid complications associated with strain hardening. Two methods to do this have been developed by Mayo and Nix.[53,54,55] In one technique, a series of indentations is made at various loading rates, and a stress and strain rate are determined for each test at a particular depth.[53,54] Figure 40 shows the results of such measurements for coarse-grained samples of Pb and Sn and for a fine-grained sample of a Pb-Sn alloy. The slopes of these curves indicate the stress exponent for creep flow, which is the reciprocal of the strain-rate sensitivity. We see that the superplastic Pb-Sn alloy has a high strain-rate sensitivity of about 0.5; by comparison, the coarse-grained samples of Pb and Sn have much lower strain-rate sensitivities.

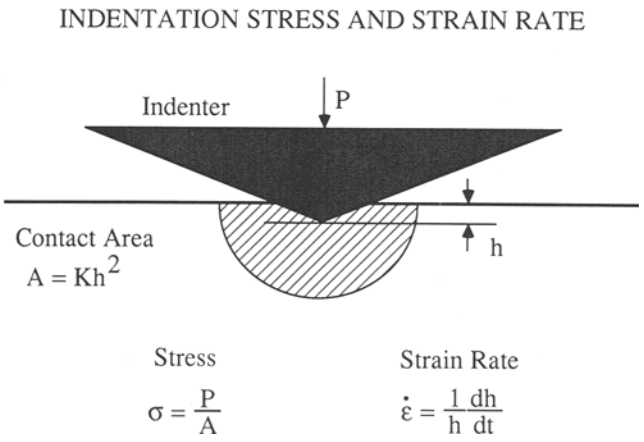

Fig. 39—Definitions of nominal stress and strain rate used in the study of strain-rate effects in indentation.

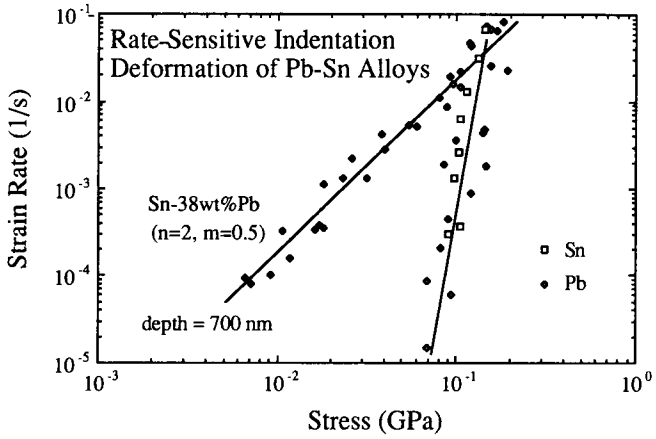

Fig. 40—Strain rate–stress relations for coarse-grained Pb and Sn and for fine-grained (superplastic) samples of a Pb-Sn alloy obtained through indentation experiments.[53,54] The indentation measurements give a high strain-rate sensitivity for fine-grained Pb-Sn, as expected. These data were obtained by making various indentations at different loading rates and measuring the stress and strain rate at a particular depth.

These results are in good agreement with tests on bulk samples of these materials. An alternate method for determining the stress exponent (or strain-rate sensitivity) has been developed recently and used for the study of strain-rate sensitivity of nanophase TiO_2.[55] In this technique, the rate of movement of the indenter into the material is monitored, while the load is held fixed after a rapid initial load application. The nominal stresses and strain rates produced in superplastic Pb-Sn using this technique are shown in Figure 41. Again we see that a high strain-rate sensitivity of 0.5 is correctly found for this material. These methods can also be used to study the strain-rate sensitivity of plastic flow in thin films, provided the strain-rate sensitivity is manifested at room temperature where the Nanoindenter can be used. Tests of this kind should provide additional information about the controlling mechanisms of deformation in thin films.

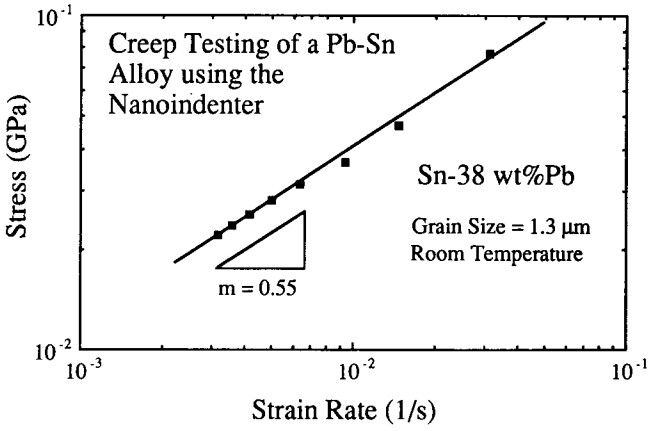

Fig. 41—Stress–strain rate relations obtained for fine-grained Pb-Sn using the Nanoindenter in the creep mode.[55] The data were taken from one indentation experiment in which the load was quickly applied and the stress and strain rate measured as the indenter sinks into the sample.

VIII. MECHANICAL TESTING OF THIN FILMS USING MICROBEAM DEFLECTION TECHNIQUES

Although the elastic and plastic properties of thin films can be studied most easily using the Nanoindenter in the indentation mode, this mode of testing has the disadvantage that the material being deformed is under a large hydrostatic pressure. In the case of porous materials, this pressure can cause densification to occur and in other cases, phase transformations can be induced. These complications sometimes make it difficult to study the elastic and plastic properties alone. To avoid the problems associated with indenter pressure, Weihs *et al.*[56,57] and Hong *et al.*[58] have developed techniques for creating micromechanical test samples in the shape of singly supported cantilever beams.

A. *Microbeam Fabrication*

The beams are typically 1 μm thick, 20 μm wide, and 50 to 100 μm long. Lithographic patterning and anisotropic etching (or chemical micromachining) techniques are used to make these structures. Once fabricated, the beams are tested in the bending mode using the Nanoindenter. Both elastic and plastic deformation of thin film materials can be studied in this way. Because the deformation occurs mainly at the fixed end of the beam, it is not affected by the pressure under the indenter. Figures 42 and 43 show scanning electron micrographs of microbeams of SiO_2 and Au, respectively, made in this way. The clean faces of the pit in the silicon wafer are produced by anisotropic etching effects. The side faces of the pit are {111} planes with edges along the bottom of the pit that are parallel to the ⟨110⟩ directions. The crystallographic nature of the pit for the gold beams is shown schematically in Figure 44.

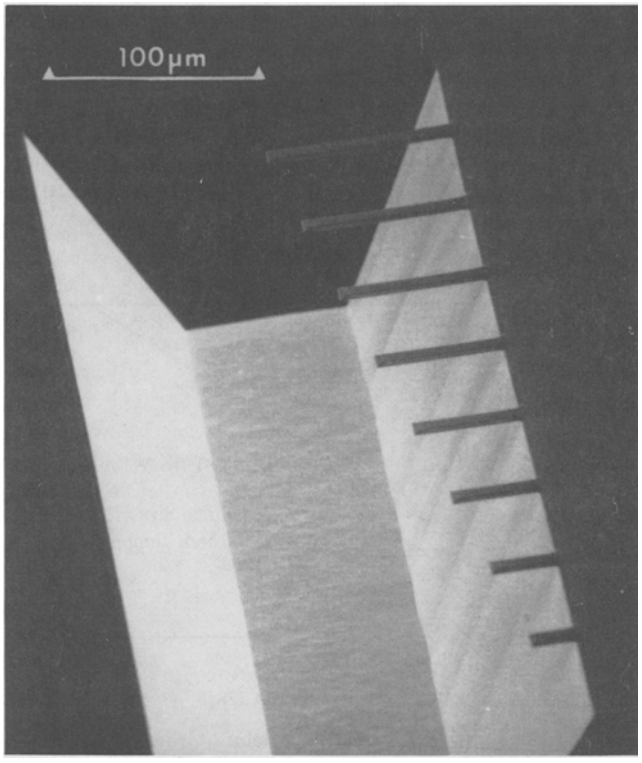

Fig. 42 — Scanning electron micrograph of cantilever microbeams of thermal SiO_2 made by integrated processing techniques.[56,57,58] The beams extend over a pit in the underlying Si substrate.

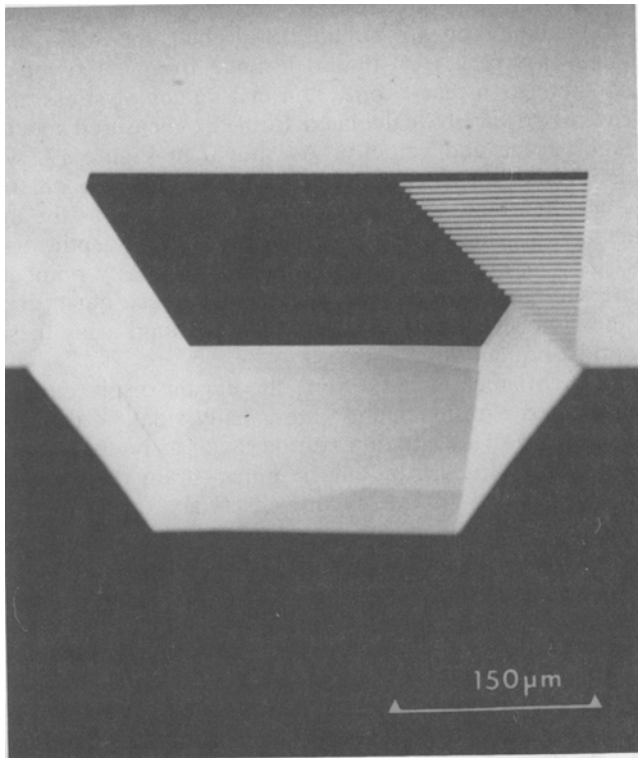

Fig. 43 — Scanning electron micrograph of cantilever microbeams of Au made by integrated processing techniques.[56,57,58] The beams extend over a pit in the underlying Si substrate.

B. *Microbeam Testing*

The testing of the microbeams is accomplished by deflecting the beams with the Nanoindenter, as shown in Figure 45. The indenter is first positioned over one point on the microbeam and then moved toward the beam by gradually increasing the force. Before the indenter contacts the beam, the imposed force is supported entirely

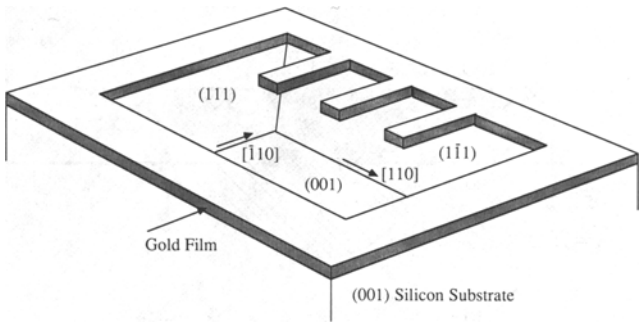

Microbeam Test Samples

Fig. 44 — Schematic diagram of microbeams of Au extending over an etch pit in the underlying Si substrate. The crystallographic orientation of the pit is created by anisotropic etching of Si.

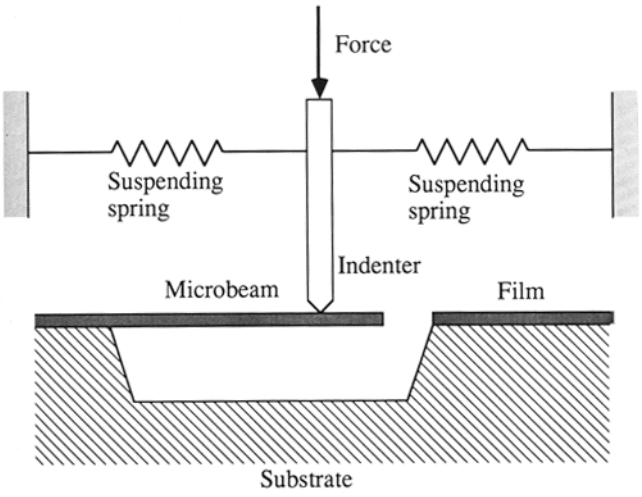

Fig. 45—Schematic diagram of the microbeam testing procedure. The indenter is placed over the beam and gradually lowered until contact with the beam is made. After contact is made, the imposed force is supported by both the suspending springs and the deflection of the microbeam.

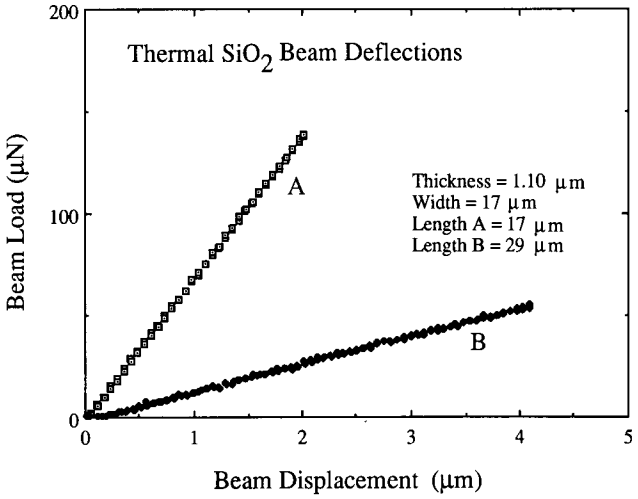

Fig. 47—Net load and net displacement measured for two deflections of a thermal SiO_2 cantilever microbeam.[56] The data shown here were taken from Fig. 46.

by the suspending springs of the Nanoindenter, and the relationship between the force and displacement in this regime is determined by the stiffness of these springs. The stiffness of the system increases as soon as the indenter makes contact with the beam. This is shown in Figure 46 for a test on a microbeam of SiO_2. In order to obtain the bending properties of the beam, it is necessary to subtract the forces associated with the deflection of the suspending springs and to measure displacement from the point at which the indenter first makes contact with the beam. When this is done for microbeams of SiO_2, the force-displacement relations shown in Figure 47 are found.

1. *Elastic properties*

The slopes of the lines in Figure 47 give the stiffnesses of the beams, and from these measurements, the elastic modulus of the beam material can be obtained, using appropriate beam bending relations and the dimensions of the beams. The elastic properties of several thin film materials found using the beam bending technique are shown in Table I and are compared with elastic properties obtained from indentation measurements. The beam bending results are in better agreement with values taken from the literature than are the indentation results.

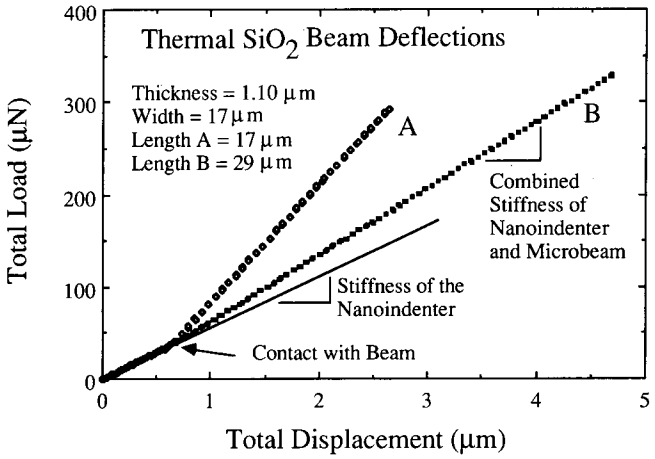

Fig. 46—Total applied load and total displacement measured for two deflections of a thermal SiO_2 cantilever microbeam.[56]

2. *Plastic properties*

The yield strengths of thin metal films can also be measured using the beam bending technique. Beam bending force-displacement relations for microbeams of gold are shown in Figure 48. The curve that starts at the origin represents the force-displacement relation associated with an initial loading and unloading of a beam. The loading curve is approximately linear, except at the highest loads where some nonelastic behavior is noted. We also see that the displacement does not return to zero when the load is completely removed. This indicates that plastic deformation occurred during the test, most likely near the substrate support where the bending stresses in the beam are maximum. A subsequent loading experiment is also shown in the figure; for clarity, the second curve has been displaced arbitrarily along the displacement axis. Note that the loading portion of the second curve remains linear up to about 60 μN, the maximum load reached in the first loading cycle. Nonlinear, plastic behavior is observed only at higher loads. This indicates that the beam was strain hardened during the first loading cycle. The increased amount of plastic deformation that occurs during the second loading cycle is indicated by the greater offset observed when the load is reduced to zero. The yield strengths and the strain-hardening properties of metal beams can be found by calculating the stresses in the beam during the course of nonelastic bending. The yield strength of thin film gold obtained in this way is shown in Table I and can be compared with the hardness of the same material obtained using indentation. We note that the yield strength of gold measured by beam bending is about $^1/_3$ of the hardness measured by indentation, a result consistent with the classical plasticity relation, $H = 3\sigma_y$.

Table I. Elastic and Plastic Properties Measured for Thin Film Coatings*

	Beam Test		Indentation Test		Literature
	Young's Modulus	Yield Strength	Young's Modulus	Hardness	Young's Modulus
Si	163	>3.39	188	13	169
Thermal SiO_2	64	>0.57	85	12	57, 66
Low temperature oxide	44	—	83	10	—
Au	57	0.34	74	1.0	39 to 78, 80**

*All data in GPa.
**First range is from measurements on thin films; second value is for bulk gold. Gold is electron-beam deposited.

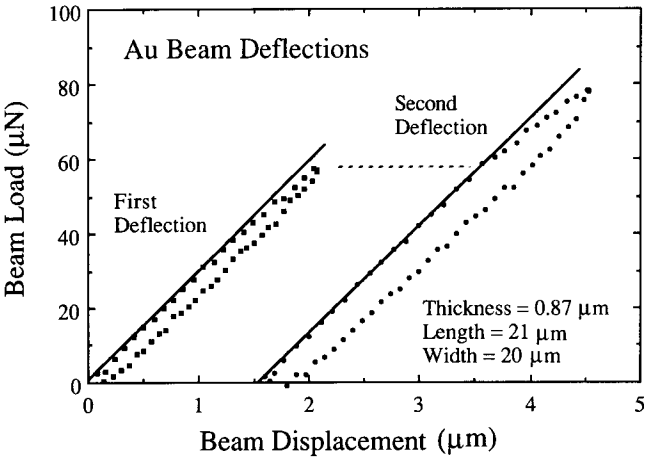

Fig. 48—Net load and net displacement measured for cantilever microbeams of Au.[56] The data from two different deflections are shown. A small amount of plastic flow occurs during the first deflection, and the beam is strain hardened. A higher load is required to cause yielding during the second deflection.

IX. CONCLUDING REMARKS

We have described the stresses in thin films on substrates, as well as some of the mechanisms by which thin film deformation occurs. This study leads to an understanding of the formation of misfit dislocations in heteroepitaxial structures and the high strengths of thin metal films on substrates. Because nontraditional testing techniques are required, much of the attention of this paper has been focused on these techniques. We have shown that laser scanning techniques for measuring substrate curvature provide a convenient way to study the biaxial stresses in thin films and the deformation processes that occur at high temperatures. Submicron indentation testing techniques for studying the hardness, elastic modulus, and time-dependent deformation properties of thin films on substrates have also been described. We have shown that the elastic and plastic properties of thin films can be studied by deflecting cantilever microbeams made by integrated circuit manufacturing methods.

The motivation for much of the work described here has been the desire to understand the mechanical properties of the thin film materials used in microelectronic and magnetic devices. As such, the work may seem to be a move away from the traditional field of mechanical properties of structural, load-bearing materials. While the experimental techniques described here may appear to be specific to the problems that arise in microelectronic and magnetic applications, they are equally useful in the study of bulk structural materials. It is important to remember that high-performance structural materials, like electronic materials, are also finely structured. There is a need to obtain information about the mechanical properties of individual features in the microstructures of structural materials. The techniques that are available for the study of microelectronic and magnetic thin films can also be used to study the mechanical properties of some of these microstructural features. In this way, the study of mechanical properties of thin films is complementary to the study of bulk structural materials. Thus, the mechanical properties of thin films represent but another chapter in the long history of the study of the relationship between microstructure and mechanical properties in the field of Metallurgy and Materials Science.

ACKNOWLEDGMENTS

The author is pleased to acknowledge the support and encouragement he has received from friends and colleagues in connection with the presentation of the Mehl Lecture and the preparation of this resulting manuscript. As noted in the Dedication, the late Professor G. Marshall Pound provided inspiration that influenced the present work even though the work itself was done in his absence. Current Stanford University faculty who contributed significantly to the present work include Professor D.M. Barnett, who provided solutions for dislocations in thin films on substrates; Professor P.A. Flinn, who built the wafer curvature apparatus at Stanford and inspired us to use it in our research; and Professor J.C. Bravman, who collaborated with us in the work on microbeams and provided much needed help in the preparation of the lecture and this manuscript. Many present and former Ph.D. students have also contributed to this work. Most notable among these are Dr. M.F. Doerner of IBM, San Jose, who was the first of my students to study the mechanical properties of thin films, and T.P. Weihs, who has continued that work and has innovated other Nanoindenter testing methods. Other students and former students who have contributed to this work and have helped with the preparation of this manuscript include Dr. M.J. Mayo, Dr. A.K. Bhattacharya, S.P. Baker, S. Hong, D. Noble, J.F. Turlo, and A.I. Sauter. The help of all of these colleagues is very much appreciated. The editorial assistance of J.A. Nix is also acknowledged and appreciated. The financial support of the Air Force Office of Scientific Research under AFOSR Grant No. 89-0185 and the Defence Research Projects

Agency through the University Research Initiative Program at the University of California, Santa Barbara under ONR Contract No. N00014-86-K-0753 is gratefully acknowledged.

REFERENCES

1. G.E. Henein and W.R. Wagner: *J. Appl. Phys.*, 1983, vol. 54, pp. 6395-6400.
2. K. Roll: *J. Appl. Phys.*, 1976, vol. 47, pp. 3224-29.
3. P.H. Townsend, D.M. Barnett, and T.A. Brunner: *J. Appl. Phys.*, 1987, vol. 62, pp. 4438-44.
4. J.H. van der Merwe: *J. Appl. Phys.*, 1963, vol. 34, pp. 123-27.
5. J.W. Matthews and A.E. Blakeslee: *J. Cryst. Growth*, 1974, vol. 27, pp. 118-25.
6. J.W. Matthews and A.E. Blakeslee: *J. Cryst. Growth*, 1975, vol. 29, pp. 273-80.
7. J.W. Matthews: *J. Vac. Sci. Technol.*, 1975, vol. 12, pp. 126-33.
8. E. Kaspar and H.-J. Herzog: *Thin Solid Films*, 1977, vol. 44, pp. 357-70.
9. J.C. Bean, L.C. Feldman, A.T. Fiory, S. Nakahara, and I.K. Robinson: *J. Vac. Sci. Technol. A*, 1984, vol. 2, pp. 436-40.
10. J.Y. Tsao, B.W. Dodson, S.T. Picraux, and D.M. Cornelison: *Phys. Rev. Lett.*, 1987, vol. 59, pp. 2455-58.
11. C. Gronet: Ph.D. Dissertation, Stanford University, Stanford, CA, 1988.
12. Y. Kohama, Y. Fukuda, and M. Seki: *Appl. Phys. Lett.*, 1988, vol. 52, pp. 380-82.
13. P.L. Gourley, I.J. Fritz, and L.R. Dawson: *Appl. Phys. Lett.*, 1988, vol. 52, pp. 377-79.
14. P.M.J. Maree, J.C. Barbour, J.F. van der Veen, K.L. Kavanagh, C.W.T. Bulle-Lieuwma, and M.P.A. Viegers: *J. Appl. Phys.*, 1987, vol. 62, pp. 4413-20.
15. R. Hull, J.C. Bean, D.J. Werder, and R.E. Leibenguth: *Appl. Phys. Lett.*, 1988, vol. 52, pp. 1605-07.
16. B.W. Dodson and J.Y. Tsao: *Appl. Phys. Lett.*, 1987, vol. 51, pp. 1325-27.
17. L.B. Freund: *J. Appl. Mech.*, 1987, vol. 54, pp. 553-57.
18. D.M. Barnett: Stanford University, Stanford, CA, private communication, 1987.
19. P. Haasen and H. Alexander: *Solid State Physics*, 1968, vol. 22, pp. 27-158.
20. H. Steinhardt and S. Schafer: *Acta Metall.*, 1971, vol. 19, pp. 65-70.
21. H. Steinhardt and P. Haasen: *Phys. Status Solidi A*, 1978, vol. 49, pp. 93-101.
22. W. Hagen and H. Strunk: *J. Appl. Phys.*, 1978, vol. 17, pp. 85-87.
23. K. Rajan and M. Denhoff: *J. Appl. Phys.*, 1987, vol. 62, pp. 1710-16.
24. P.A. Flinn, D.S. Gardner, and W.D. Nix: *IEEE Trans. on Electron Devices*, 1987, vol. ED-34, pp. 689-99.
25. M.F. Doerner and S. Brennan: *J. Appl. Phys.*, 1988, vol. 63, pp. 126-31.
26. P.H. Townsend: Ph.D. Dissertation, Stanford University, Stanford, CA, 1987.
27. D.S. Gardner, T.L. Michalka, P.A. Flinn, T.W. Barbee, Jr.: K.C. Saraswat, and J.D. Meindl: *Proc. 2nd Int. IEEE VLSI Multilevel Interconnection Conf.*, 1985, pp. 102-10.
28. T.S. Kuan and M. Murakami: *Metall. Trans. A*, 1982, vol. 13A, pp. 383-91.
29. M.F. Doerner, D.S. Gardner, and W.D. Nix: *J. Mater. Res.*, 1986, vol. 1, pp. 845-51.
30. M.F. Doerner: Ph.D. Dissertation, Stanford University, Stanford, CA, 1987.
31. N. Hansen: *Acta Metall.*, 1977, vol. 25, pp. 863-69.
32. R.W. Armstrong: in *Advances in Materials Research*, H. Herman, ed., Interscience, New York, NY, 1970, vol. 4, pp. 101-46.
33. A.J. Griffin, Jr., F.R. Brotzen, and C. Dunn: *Scripta Metall.*, 1986, vol. 20, pp. 1271-72.
34. A.J. Griffin, Jr., F.R. Brotzen, and C. Dunn: *Thin Solid Films*, 1987, vol. 150, pp. 237-44.
35. M. Nishibori and K. Kinosita: *Thin Solid Films*, 1978, vol. 48, pp. 325-31.
36. D. Newey, M.A. Wilkins, and H.M. Pollock: *J. Phys. E*, 1982, vol. 15, pp. 119-22.
37. J. Pethica, R. Hutchings, and W.C. Oliver: *Phil. Mag.*, 1983, vol. A48, pp. 593-606.
38. J.L. Loubet, J.M. Georges, J.M. Marchesini, and G. Meille: *J. Tribol.*, 1984, vol. 106, pp. 43-48.
39. P.E. Wierenga and A.J.J. Franken: *Philips Tech. Rev.*, 1985, vol. 42, pp. 85-92.
40. H. Bangert, A. Kaminitschek, A. Wagendristel, A. Barna, P.B. Barna, and G. Radnoczi: *Thin Solid Films*, 1986, vol. 137, pp. 193-98.
41. S.-P. Hannula, D. Stone, and C.-Y. Li: *Mater. Res. Symp. Proc.*, 1985, vol. 40, pp. 217-24.
42. D. Stone, W.R. LaFontaine, P. Alexopoulous, T.-W. Wu, and C.-Y. Li: *J. Mater. Res.*, 1988, vol. 3, pp. 141-47.
43. J.B. Pethica and W.C. Oliver: *Mater. Res. Symp. Proc.*, 1989, vol. 130, pp. 13-23.
44. D. Stone, W. LaFontaine, S. Ruoff, and C.-Y. Li: *Mater. Res. Soc. Proc.*, 1986, vol. 72, pp. 43-49.
45. H.-Y. Yu and J.C.M. Li: *J. Mater. Sci.*, 1977, vol. 12, pp. 2214-22.
46. H.-Y. Yu, M.A. Imam, and B.B. Rath: *J. Mater. Sci.*, 1985, vol. 20, pp. 636-42.
47. H.-Y. Yu, S.C. Sanday, and B.B. Rath: *Naval Research Laboratory Report*, Report No. 9168, Naval Research Laboratory, Washington, DC, Jan. 12, 1989.
48. M.F. Doerner and W.D. Nix: *J. Mater. Res.*, 1986, vol. 1, pp. 601-09.
49. I.N. Sneddon: *Int. J. Eng. Sci.*, 1965, vol. 3, pp. 47-62.
50. R.B. King: *Int. J. Solids Struct.*, 1987, vol. 23, pp. 1657-64.
51. T.F. Page, W.C. Oliver, and C.J. McHargue: *J. Mater. Sci.*, in press.
52. A.K. Bhattacharya and W.D. Nix: *Int. J. Solids Struct.*, 1988, vol. 24, pp. 1287-98.
53. M.J. Mayo and W.D. Nix: *Acta Metall.*, 1988, vol. 36, pp. 2183-92.
54. M.J. Mayo and W.D. Nix: *Proc. 8th Int. Conf. on Strength of Metals and Alloys*, Tampere, Finland, P.O. Kettunen, T.K. Lepisto, and M.E. Lehtonen, eds., Pergamon Press, Oxford, 1988, pp. 1415-20.
55. M.J. Mayo: Sandia National Laboratories, Albuquerque, NM, unpublished research, 1989.
56. T.P. Weihs, S. Hong, J.C. Bravman, and W.D. Nix: *J. Mater. Res.*, 1988, vol. 3, pp. 931-42.
57. T.P. Weihs, S. Hong, J.C. Bravman, and W.D. Nix: *Mater. Res. Symp. Proc.*, 1989, vol. 130, pp. 87-92.
58. S. Hong, T.P. Weihs, J.C. Bravman, and W.D. Nix: *Mater. Res. Symp. Proc.*, 1989, vol. 130, pp. 93-98.